# A critical review of heat and mass transfer correlations for LiBr-H₂O and NH₃-H₂O absorption refrigeration machines using falling liquid film technology

Beethoven Narváez-Romo [a], Marx Chhay [b], Elí W. Zavaleta-Aguilar [c], José R. Simões-Moreira [a,*]

[a] SISEA-Alternative Energy Systems Laboratory, Av. Professor Mello Moraes, 2231 - Cidade Universitária, São Paulo, Brazil
[b] LOCIE-Laboratoire Optimisation de la Conception et Ingénierie de l'Environnement, Université Savoie Mont Blanc, 73376 Le Bourget-du-Lac, France
[c] São Paulo State University (Unesp), Campus of Itapeva, Rua Geraldo Alckmin, 519, 18409-010 Itapeva, São Paulo, Brazil

## HIGHLIGHTS

- A review of heat and mass transfer correlations based on falling film is showed.
- Heat and mass transfer correlations (Nu, Sh) are summarized.
- Non-dimensional (Nu, Sh) mapping for refrigeration and air-conditioning are showed.

## ARTICLE INFO

## ABSTRACT

This paper presents an extensive review of heat and mass transfer correlations in the framework of sorption machines operating based on the falling film technology, in which ammonia-water and lithium bromide-water are used as the working fluid pairs. Heat and mass transfer correlations are summarized as well as the application range and geometrical configuration. In order to compare the correlations found in the recent and classical literature, typical operation conditions for absorption refrigeration cycles have been adopted. Heat and mass transfer correlations have been evaluated for both working fluid pairs, mapping the possible heat and mass transfer values for refrigeration and air-conditioning applications. The study allowed comparing the two technologies using the same operational conditions. The ascertainment that the transfer correlations may behave differently has been showed. Finally, this work suggests that future researches about heat and mass transfer behavior should be to carry out for realistic operational condition of the absorption refrigeration cycles.

## Contents

---

* Corresponding author at: SISEA/Mechanical Engineering Department/Escola Politécnica, University of São Paulo, Av. Professor Mello Moraes, 2231, CEP: 05508-900, São Paulo, Brazil.
    E-mail address: jrsimoes@usp.br (J.R. Simões-Moreira).

## Nomenclature

| | |
|---|---|
| $A$ | area ($m^2$) |
| $Ar$ | Archimedes number, $Ar = D^3 g / v^2$ (–) |
| $c_p$ | specific heat at constant pressure, ($J\,kg^{-1} \circ C^{-1}$) |
| $D$ | diameter (m) |
| $D^*$ | dimensionless diameter, $D^* = D/L_c$ (–) |
| $D_h$ | hydraulic diameter (m) |
| $D_m$ | mass diffusivity ($m^2\,s^{-1}$) |
| $\dot{m}$ | mass flow rate ($kg\,s^{-1}$) |
| $\dot{q}$ | heat rate (W) |
| ln | neperian logarithm (–) |
| $e$ | Euler's number (–) |
| $E_T$ | Ackermmn's correction factor, Eq. (4) (–) |
| $f$ | fouling factor (–) |
| $g$ | acceleration of gravity ($m\,s^{-2}$) |
| $Ga$ | Galileu number, $Ga = 1/Ka$ (–) |
| $Gr$ | Grashof number $Gr = g\beta_T(T_w - T)/v^2$ (–) |
| $h$ | heat transfer coefficient ($W\,m^{-2} \circ C^{-1}$) |
| $h^*$ | corrected heat transfer coefficient ($W\,m^{-2} \circ C^{-1}$) |
| $i$ | specific enthalpy ($J\,kg^{-1}$) |
| $i_{lv}$ | vaporization enthalpy ($J\,kg^{-1}$) |
| $ID$ | internal diameter (m) |
| $Ja$ | Jakob number, $c_p(T_w - T_{sat})/\Delta i_{vap}$ (–) |
| $k$ | thermal conductivity ($W\,m^{-1} \circ C^{-1}$) |
| $k_m$ | mass transfer coefficient Kmol $m^{-2}\,s^{-1}$) |
| $Ka$ | Kapitza number, $Ka = g\mu^4/\rho\sigma^3$ (–) |
| $L$ | length (m) |
| $L_c$ | characteristic length or viscous length scale, $L_c = (v^2/g)^{1/3}$ (m) |
| $Le$ | Lewis number, $Le = Sc/Pr$ (–) |
| $M_m$ | molecular weight ($kg\,kmol^{-1}$) |
| $N$ | tube number (–) |
| $Nu$ | Nusselt number, $Nu = hL_c/k$ (–) |
| $OD$ | outlet diameter (m) |
| $P$ | pressure (kPa) |
| $P_{wet}$ | wet perimeter (m) |
| $ppm$ | parts per million |
| $Pr$ | Prandtl number $Pr = c_p\mu/k$ (–) |
| $q''$ | heat flux ($[W\,m^{-2}$) |
| $Re$ | Reynolds number, $Re = 4\Gamma/\mu$ (–) |
| $S$ | tube spacing (m) |
| $s^*$ | dimensionless vertical tube spacing $s^* = S/D\,L_c$ (–) |
| $Sc$ | Schmidt number $Sc = v/D_m$ (–) |
| $Sh$ | Sherwood number, $Sh = k_m L_c/D_m$, (–) |
| $T$ | temperature (°C) |
| $U$ | global heat transfer coefficient ($W\,m^{-2} \circ C^{-1}$) |
| $V$ | velocity ($m\,s^{-1}$) |
| $W$ | width (m) |

| | | |
|---|---|---|
| $x$ | concentration-liquid, ($kg_{comp.}\,kg_{solution}^{-1}$) | $x = m_{comp.}/m_{solution}$, |
| $y$ | concentration-vapor, ($kg_{comp.}\,kg_{solution}^{-1}$) | $x = m_{comp.}/m_{solution}$, |
| ARC | Absorption Refrigeration Cycle (–) | |
| COP | coefficient of performance (–) | |
| VCC | vapor compression cycle (–) | |
| EH | ethyl hexanol | |
| EV | expansion valve (–) | |
| Li-Br | lithium bromide | |
| OSF | offset strip fins (–) | |

*Greek symbols*

| | |
|---|---|
| $\Delta T$ | temperature difference (–) |
| $\Delta x$ | concentration difference (–) |
| $\beta$ | tilt angle of the flat plate (°) |
| $\beta_T$ | coefficient of thermal expansion ($K^{-1}$) |
| $\delta$ | film thickness (m) |
| $\Gamma$ | mass flow rate per unit length on each side ($kg\,s^{-1}\,m^{-1}$) |
| $\mu$ | dynamic viscosity ($kg\,m^{-1}\,s^{-1}$) |
| $v$ | kinematic viscosity ($m^2\,s^{-1}$) |
| $\rho$ | density, ($kg\,m^{-3}$) |
| $\tau_v^*$ | non-dimensional shear stress (–) |
| $\theta$ | tube angle or wettability of the tube (°) |

*Subscripts*

| | |
|---|---|
| abs | absorber/absorption (–) |
| b | bulk (–) |
| c | cooling/coolant (–) |
| con | condenser/condensation (–) |
| conv | convective (inner of the tube) (–) |
| eq | equilibrium (–) |
| eva/vap | evaporator/evaporation (–) |
| i | inlet (–) |
| int | interface (–) |
| l | liquid (–) |
| lm | logarithmic mean (–) |
| o | outlet (–) |
| rect | rectifier (–) |
| seg | segmented (–) |
| ss | strong solution (–) |
| sub | subcooling (–) |
| v | vapor (–) |
| w | wall (–) |
| ws | weak solution (–) |

## 1. Introduction

Edmond Carré developed the first absorption refrigeration machine in 1850 using a water and sulphuric acid ($H_2SO_4$) mixture as the working fluid pair, requiring a large quantity of this acid to absorb a small quantity of water vapor in order to achieve the refrigeration process. However, in 1859, Ferdinand Carré used the ammonia-water pair as working fluid, because of its properties: stability, low normal boiling point (44 °C), and good ammonia affinity to water [1]. Currently, lithium bromide-water and ammonia-water pairs have been the most common working fluid pairs used in commercial absorption refrigeration cycles (ARC). The former operates in vacuum such as in Edmond Carré's machine, and the second one in a positive pressure such as in Ferdinand Carré 's machine.

An ARC is constituted by two pressure levels as depicted in Fig. 1; the low pressure level (evaporator and absorber) and the high pressure level (generator and condenser). These two levels are connected by two expansion valves (EV1 and EV2) and one solution pump, in its simplest configuration. The solution pump drives the strong liquid solution from the absorber to the generator in ammonia-water technology (or the weak liquid solution for the lithium bromide-water technology). At the generator, the solution flows over heated surface in the falling film generator, whose function is to separate the refrigerant (ammonia or water vapor) from the liquid solution. Next, the vapor refrigerant is driven to the condenser, rejecting the heat to the environment, $\dot{Q}_{con}$. The condensed refrigerant reaches the evaporator, going through an expansion valve (EV2) reducing the pressure and the temperature by the Joule-Thomson effect to receive the heat load ($\dot{Q}_{eva}$) by evaporation process. Next, the vapor refrigerant enters the absorber at the vapor state, in which it is absorbed by the weak solution (or strong for lithium bromide-water technology). Heat ($\dot{Q}_{abs}$) is rejected to an external coolant as the absorption process takes place, and then the solution is pumped to the generator closing the cycle.

It is worth mentioning that both the absorber and the generator are the main components of the absorption system because that there is a simultaneous heat and mass transfer process [2], in which the refrigerant changes phase [3]. In addition, the heat and mass transfer coefficients in those components are characterized by low values [4]. On the other hand, when ARC is compared with a vapor compression cycle (VCC), the former has lower coefficient of performance (COP), particularly if the absorption machine works beyond its design specifications, e.g. the vaporization temperature, or the cooling thermal load, due to a problem of partial evaporation at the evaporator. Additionally, the COP is also sensitive to the heat source temperature in the desorber, the cooling temperature of the evaporator, and flow rate of the strong solution. Therefore, enhancing the heat and mass transfer process leads to a reduction in costs and in the sorption machine size.

Although the technical development of such machines has reached an acceptable maturity for industrial purpose, research is still active as more experimental work and theoretical analysis are necessary. For example, one of the challenging consists in reducing electrically consumption and increasing the compactness of sorptions machines in order to integrate them into other environment (high efficiency buildings, transport, solar drive machines, to mention a few new applications). The conception of new technologies implies appropriate sizing rules, depending on the transfer mechanisms. Thus, a comprehensive review of transfer correlations, including their comparison into a realistic ARC system framework, is still relevant. The literature review is hitherto focused on some specific category of study: Thome [5] carried out a review of falling film evaporation on both smooth and enhanced tubes focusing on working fluids as alternative refrigerants including ammonia; he found that the falling film technology provides a higher heat transfer coefficient than flooded evaporators. Killion and Garimella [6] carried out a complete critical review on falling film technology in absorption processes, in which these efforts are focused analyzing the mathematical model that have been used to the simultaneous heat and mass transfer processes. Ribatski and Jacobi [7] carried out a critical review of falling film evaporation process over horizontal tubes (single and tube bundles), covering hydrodynamic studies and the heat transfer coefficient affected by several operation conditions on smooth and enhanced tubes. They pointed out that the falling film technology presents inconveniences due the liquid film maldistribution and dry-out problems. However, the installation of a wire mesh over the distributor homogenized the liquid flow and guaranteed the total wettability over the first tube [8]. Prost et al. [9] analyzed the heat transfer behavior falling film evaporator under several operation conditions for the food industry. They reported some Nusselt number correlations from the literature. Narváez-Romo and Simões-Moreira [10] carried out a literature review of falling film evaporation, studying the parameters affecting the heat transfer coefficient. Tomforde and Luke [11] carried out a literature review on falling film absorbers focused on horizontal tubes only, in which lithium bromide-water, and R134a-Dimethylacetamide (DMAC) were the working fluid pairs studied.

The present work aims to emphasize the agreement between numerical and experimental studies based on the correlations that researchers have obtained. All correlations for heat and mass transfer in falling film technology are carried out for sorption process using the two most common working commercial fluid pairs: ammonia-water and lithium bromide-water. The comparisons are summarized in Tables 2 and 3 for ammonia-water studies, and in Tables 5 and 6 for lithium bromide-water studies: a straightforward observation shows the lack of analytical/numerical results for transfer correlations using ammonia-water solution. Furthermore, in contrast with the existing literature, the final section of the present work is devoted to an application of the presented transfer correlations into realistic ARC systems. This original performance aims to highlight that the use of transfer correlations for optimizing ARC systems may not be straightforward, due to the differences of behavior obtained (see Section 6) The present work is organized as follows: in the first place, a review of the mean definition correlations and the classical hypothesis assumed to compute the heat and mass transfer coefficients are presented. Next sections, the transfer correlations involving ammonia-water solution and lithium bromide-water systems are discussed, in which each one is classified by application (absorption or desorption) and
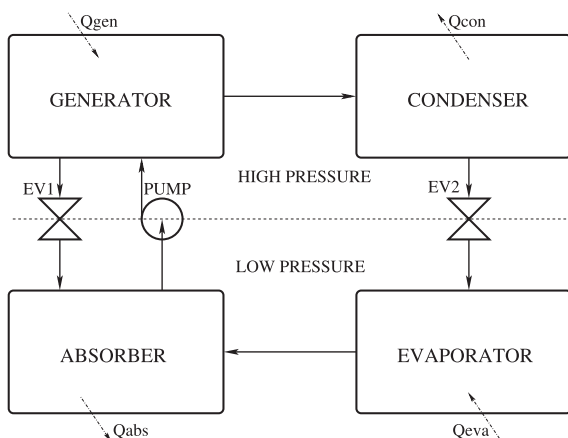


Fig. 1. ARC diagram.

**Table 1**
Mass flow rate per unit length for various geometries.

| $\Gamma$, kg m$^{-1}$ s$^{-1}$ | Geometry |
|---|---|
| $\frac{\dot{m}}{2W}$ | Horizontal tube or flat plate (both sides wet) |
| $\frac{\dot{m}}{W}$ | Flat plate (one side wet) |
| $\frac{\dot{m}}{\pi D}$ | Vertical tube |

**Table 4**
Constant for Eqs. (44) and (45) ($\times 10^{-3}$).

| Configuration | a | b | c | d |
|---|---|---|---|---|
| Solution, Bare | 24.9 | 69 | 896 | −300 |
| Solution, Screen | 4.93 | 469 | 965 | −343 |
| Solution +2-EH, Bare | 25.9 | 247 | 2623 | −265 |
| Solution +2-EH, Screen | 16.6 | 279 | 886 | −240 |

geometry disposal. Additionally, these correlation are summarized in tables by application range and by test rig specifications. Next, others relevant falling film studies are showed, whose working fluid are different to the current study, but these have been used in ARC researches. Finally, the heat and mass transfer

mapping of these correlations are carried out in a realistic operational conditions of an ARC for refrigeration (−20 °C) and airconditioning (7 °C) applications. Also, the study aims to compare the heat and mass transfer correlations, looking for a standardization comparison for further studies, due that, currently, there

**Table 2**
Application range of the correlations using ammonia-water.

| Author | Correlation | Pr | Re | Sc | T, °C | P, kPa | x, % y, % | Remarks |
|---|---|---|---|---|---|---|---|---|
| *Falling film Absorber using Ammonia-Water solution* | | | | | | | | |
| Bohra [31] | (25), (26) | 2.2–10.4 | 26–157 | 45.4–588.1 | 14.8–105.4 | 169–520 | 5; 15; 25; 40 | |
| | | 0.5–0.93 | – | 0.5–0.53 | (−10.5)–28.2 | | – | |
| Jeong et al. [15] | 34 | 2.4–3.9 | 20–300 | – | 45–54 | 67–117 | 1.2; 3.7 | |
| | | – | – | | 66–69 | | 63; 77 | |
| Kang et al. [27] | (30) and (31) | 3.8–5.8 | 17–24 | 33.8–39.2 | 17.0–37.2 | 101.3 | 5; 10; 15 | |
| | | – | – | – | 54.5–66.5 | | 64.7–79.7 | |
| Kwon and Jeong [14] | (35) and (36) | 2.1–3.8 | 10–250 | – | 45–60 | 17–193 | 3; 14; 30 | |
| | | – | – | | – | | 45.6; 84.4; 96.5 | |
| Lee [37] | (27)–(29) | 2.2–8.2 | 29.7–169.2 | 43.6–362.7 | 14.8–105.4 | 169–520 | 5; 15; 25; 40 | $Gr_v = (4.22 - 59.89) \times 10^3$ |
| | | 0.5–0.93 | – | 0.5–0.53 | (−10.5)–28.2 | | – | $Ja_v = (9.8 - 38.7) \times 10^{-3}$ |
| Lee et al. [47] | 32, 33 | 3.8–5.8 | 50–700 | | 15.5–20 | 101.3 | 0.1–0.3 | |
| | | – | 25–200 | | – | | – | |
| *Other works using Ammonia-Water solution* | | | | | | | | |
| Zavaleta-Aguilar and Simões-Moreira [36] | 37 | 1.68–2.65 | 108–246 | – | 87–103 | 1460–1611 | 37; 49 | Generator |

**Table 3**
Summary of configuration studies on absorption and generation using ammonia water.

| Author | Geometrical specifications | Compared | Comments |
|---|---|---|---|
| *Experimental works using Ammonia Water: Configuration of study* | | | |
| Bohra [31] | Horizontal tube bundle 4Cx6R<br>$O.D = 9.5 \times 10^{-3}$ m, $L = 0.29$ m, $S = 2 \times 10^{-2}$ m<br>$\delta_w = 7 \times 10^{-4}$ m $A_{total} = 0.210$ m$^2$ | Wilke [43], Dorokhov and Bochagov [48], Hu and Jacobi [49], Kwon and Jeong [14], Meacham and Garimella [50], Meacham and Garimella [51] | Water counter-current cooling and Counter-current absorption |
| Jeong et al. [15] | Coiled tube<br>$O.D = 12.7 \times 10^{-3}$ mm, $I.D = 10.7 \times 10^{-3}$ mm<br>$\overline{D_{coil}} = 82.7 \times 10^{-3}$ m | | Water co-current cooling and Counter-current absorption |
| Kang et al. [27] | Surfaces as offset strip fin stainless steel<br>$0.1 * 0.13 * 3.4 \times 10^{-2}$ mm$^3$ Fin<br>pitch = 1.95 mm, $\delta_w = 2 \times 10^{-4}$ m Fin<br>height = $4.8 \times 10^{-3}$ mm $A_{total} = 14.3 \times 10^{-3}$ m$^2$ | | Water counter-cross cooling and Co-current absorption |
| Kwon and Jeong [14] | Coiled tube<br>$O.D = 12.7 \times 10^{-3}$ mm, $I.D = 10.7 \times 10^{-3}$ mm, $L = 0.6$ m<br>$A_{total} = 2.4 \times 10^{-2}$ m$^2$ | | Water co-current cooling and Co/counter-current absorption It took into account the shear stress at the vapor-liquid interface It used the same test rig as Jeong et al. [15] |
| Lee et al. [41] | Three surface types smooth plate, hair lined plated treated by laser, and plate treated by sand paper (higher wettability)<br>$0.112 \times 0.264 \times 3 \times 10^{-4}$ m$^3$, and $A_{total} = 29.6 \times 10^{-3}$ m$^2$ | | Bubble, Water counter-current cooling Counter-current absorption |
| Lee [47] | Three surface types smooth plate, hair lined plated treated by laser, and plate treated by sand paper (higher wettability)<br>$0.112 \times 0.264 \times 3 \times 10^{-4}$ m$^3$, and $A_{total} = 29.6 \times 10^{-3}$ m$^2$ | Lee [47]: bubble tecnology | Bubble Water counter-current cooling Counter-current absorption |
| Zavaleta-Aguilar and Simões-Moreira [36] | Horizontal stainless steel tube bundle 7 Col x10Row<br>$\delta_w = 1 \times 10^{-3}$ m, $O.D = 8 \times 10^{-3}$ m, $L = 0.15$ m<br>$A_T = 26.4 \times 10^{-2}$ m$^2$ | Hu and Jacobi [49], Wilke [43], Chun and Seban [52] Mitrovic [53], Owens [54], Fujita and Tsutsui [55] | Generator-Rectifier Heating by thermal oil-Generator Water cooling-Rectifier Ammonia water. A 100% surface wettability was achieved for Re above 100 up to nearly 250 Properties by EES and Conde [56] |

**Table 5**
Application range of the correlations using lithium bromide-water.

| Author | Correlation | $Pr$ | $Re$ | $T$, °C | $P$, kPa | $x$ | Remarks |
|---|---|---|---|---|---|---|---|
| *Generator falling film using lithium bromide-water solution* | | | | | | | |
| Jani et al. [30] | 40, 41 | 7–10 | 100–500 | 60–140 | 5–10 | 50–60 | |
| Jani [57] | 42, 43 | 7–10 | 100–500 | 60–140 | 5–10 | 50–60 | $Sc = 268$ |
| Shi et al. [34] | 38 | 3.8–4.7 | $\leq 500^*$ | 126–150 | 97.25 | 49.5–58 | $q'' = 5-25$ kW/m² |
| Shi et al. [35] | 39 | 5.6–10.61 | 287–770 | 126–150 | 9.725 | 49.5–58 | $q'' = 10-25$ kW/m² |
| *Absorber falling film using lithium bromide-water solution* | | | | | | | |
| Babadi and Farhanieh [59] | (54)–(56) | 28.5 | 5–100 | 40 | 1 | 62 | |
| Karami and Farhanieh [22] | 46, 47 | 17.7 | 5–150 | 45 | 1 | 60 | |
| Karami and Farhanieh [23] | 48, 49 | 17.7 | 5–150 | 45 | 1 | 60 | Inclined plate |
| Kim and Infante-Ferreira [32] | 44, 45 | $\cong 11 - 15$ | 40–110 | 18–42 | 0.7–2.9 | 50 | |

**Table 6**
Summary of configuration studies on sorption process using lithium bromide-water.

| Author | Geometrical specifications | Compared | Comments |
|---|---|---|---|
| *Analytical and numerical works using lithium bromide: configuration of study* | | | |
| Babadi and Farhanieh [59] | Horizontal tube $D = 20 \times 10^{-3}$ m | | Method: finite difference method. Assumes the total wettability of the tube |
| Jani et al. [30] | Tube bundle $D = 19.05 \times 10^{-3}$ m, $S = 3 \times 10^{-2}$ m | Kim and Kim [61], Jani et al. [62] | Method: Non-linear differential equations solved by Runge-Kutta. The position tube effect on the row tube bundle is analyzed |
| Jani [57] | Horizontal tube $D = 19.05 \times 10^{-3}$ m | Kim and Kim [61], Shi et al. [35], Nusselt [21] | Method: implicit Crank-Nicolson method |
| Karami and Farhanieh [22] | Vertical plate $L = 1$ m | Medrano et al. [63] | Method: Fully implicit finite difference. Properties: Florides et al. [16], and McNeely [58]. Convergence criterion: mass flux ($10^{-6}$) |
| Karami and Farhanieh [23] | Incline plate $L = 1$ m | Medrano et al. [63] | Properties: Florides et al. [16], and McNeely [58]. Method: Implicit finite difference. Convergence criterion: mass flux ($10^{-6}$) |
| *Experimental works using Lithium Bromide: Configuration of study* | | | |
| Kim and Infante-Ferreira [32] | Flat plate-smooth copper surface and copper + wire screen Screen: woven with $3.8 \times 10^{-4}$ m copper wire, having 22 meshes per inch. $0.095 \times 0.540$ m $A_{total} = 51.3 \times 10^{-3}$ m² | Heat transfer: Hoffmann et al. [64] Mass transfer: Yih and Chen [65], Nagaoka et al. [66], Kim et al. [67] | Adiabatic condition are tested too. Properties: thermodynamic properties of [68] $k$, $\mu$ of [69], and $D_m$ of [70] |
| Shi et al. [34] | Vertical tube $L = 0.760$ m, $O.D = 25 \times 10^{-3}$ m | | Study with modeling |
| Shi et al. [35] | Vertical stainless steel in-tube $\delta_w = 2 \times 10^{-3}$ m, $O.D = 25 \times 10^{-3}$ m, $L = 0.76$ m | | Overall heat transfer in-tube falling film is 4.37 times higher than immersed generator |

are not a heat transfer correlation for ammonia-water falling film in absorption processes using nanoparticles [12].

## 2. Heat and mass transfer using falling films technology in sorption processes

The falling film technology can be used in different applications, such as in ARC. In this technology, there is a large heat transfer contact area between the wall surface and the liquid falling film, enhancing the heat removal for the absorption process case [2]. However, the whole heat and mass transfer resistance is concentrated in the thin liquid falling film [2,13]. Fig. 2a shows the general falling film technology on horizontal tubes and Fig. 2b the temperature and concentration profiles for the absorptions process in a vertical plate. The generation process is used for evaporation or distillation processes, in which the wall temperature ($T_w$) is higher than the liquid falling film temperature ($T_l$), allowing the phase change (pure substance entering at the saturated condition), or the separation process (no binary azeotrope substance entering at the saturated condition).

On the other hand, in the absorption process, the wall temperature ($T_w$) is lower than the liquid falling film ($T_l$), removing the heat of absorption ($\dot{Q}_{abs}$) and absorbing the vapor ($\dot{m}''_{abs}$) into the liquid falling film as shown in Fig. 2b, i.e., the heat of absorption is released at the liquid-vapor interface only, yielding an increase of the average film temperature ($T_b$), which diminishes the vapor

solubility and, therefore, the absorption rate is strongly controlled by the intensity of heat removal from the liquid falling film to the coolant ($\dot{q}_c$) [2], while $s$ and $S$ are the inter-tube distances, respectively; $T_c$, $T_{int}$ and $T_v$ are the coolant, interface, and vapor temperature, respectively; $x_b$, $x_{int}$ and $y$ are the average concentration of the liquid falling film, the concentration of the liquid falling film at the interface, and the vapor concentration, respectively;

### 2.1. Heat and mass transfer coefficient calculation

In the falling film technology, the thermal resistance analogy is used to compute the global or overall heat transfer coefficient ($U$) between the bulk solution and the cooling or heating fluid, and given by Eq. (1),

$$\frac{1}{U} = \frac{1}{h_{l,w}} + \frac{D_o}{2k_w} \ln \frac{D_i}{D_o} + \frac{D_i}{D_o h_{conv}} + f \tag{1}$$

where $h_l$ is the heat transfer coefficient on the film, $h_{conv}$ is the convective heat transfer coefficient associated to the secondary fluid, $k_w$ the tube wall thermal conductivity, $D_o$, and $D_i$, the external and internal tube diameter, and $f$ represents the fouling factor resistance ($2 \times 10^{-4}$ m² °C W$^{-1}$ [14,15] in ammonia-water pair, or $9 \times 10^{-5}$ m² °C W$^{-1}$ [16] in lithium bromide-water pair).

Heat and mass transfer coefficients cannot be directly evaluated from an experimental work. Therefore, they must be computed from measured quantities (e.g. temperature, concentra-
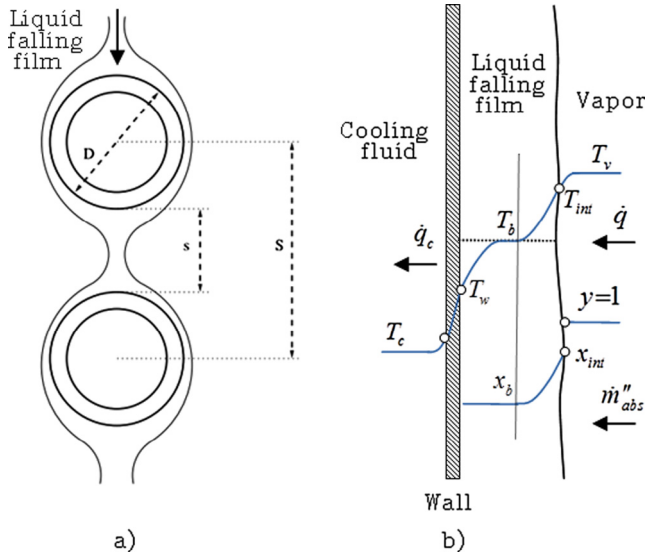
**Fig. 2.** (a) Falling film in horizontal tubes and (b) temperature and concentration profiles for the ammonia-water absorptions process in a vertical plate (adapted from [2]).

tion, liquid density) thanks to the Newton's law of cooling. This relation involves a difference in temperature, which takes into account, the wall temperature ($T_w$) and the interface temperature ($T_{int}$) in most of the cases. However, depending on how viscous sublayers are assumed both near the wall and near the liquid-vapor interface, two partial heat transfer coefficients can be defined (Fig. 2b) [2]:

- between the bulk liquid ($T_b$) and the wall ($T_w$):

$$h_{l,w} = \frac{\dot{q}_c}{T_b - T_w} \tag{2}$$

- between the liquid-vapor interface ($T_{int}$) and the bulk liquid ($T_b$):

$$h_{l,int} = \frac{\dot{m}''_{abs}\Delta i_{abs}}{T_{int} - T_b} \frac{1}{E_T} \tag{3}$$

where $E_T$ represents the Ackermmn's correction factor:

$$E_T = \frac{\Delta i_{abs}}{c_p} \frac{\ln(1 + c_p(T_{int} - T_b)/\Delta i_{abs})}{T_{int} - T_b} \tag{4}$$

in which, $\dot{q}_c$, $\dot{m}''_{abs}$ and $i_{abs}$ represent the transferred heat to the cooling fluid, the absorbed mass flow rate per area and the absorption specific enthalpy, respectively; $c_p$ is the specific heat at constant pressure. Yüksel and Schlünder [2] employed $E_T \cong 1$. Nevertheless, this approximation stands for low values of heat flow through the liquid film, hence assuming a linear profile for the temperature [13]. Thus, the average heat transfer coefficient reads:

$$\overline{h_l} = \frac{\dot{m}''_{abs}\Delta i_{abs}}{T_{int} - T_w} \tag{5}$$

The mass transfer coefficient ($k_m$) is defined by Eq. (6), while ($\rho_l$) and $P$ represent the liquid density and the system pressure, respectively

$$\overline{k_m} = \frac{\dot{m}''_{abs}}{\rho_l \ln(1 - x_b)/(1 - x_{int}(T_{int}, P))} \tag{6}$$

The use of the logarithmic mean difference is one of the most commonly used methods to compute the heat and mass transfer coefficient due to its simplicity [17]. However, Islam [18] and Fujita

and Hihara [17] show that the logarithmic mean potential occurring in the average heat and mass transfer coefficient definition (Eqs. (7) and (8)) presents wide deviations from experimental results. Due to that, the conventional method takes into account two separate processes of heat and mass transfer; the first one is the heat transfer from the liquid falling film to the cooling fluid, and the second is the absorption of refrigerant from the vapor phase to the cooling fluid, causing errors when there is not a non-linear temperature distribution of the liquid falling film in the absorber. However, the cooling fluid temperature distribution along the tube length is nearly linear [18]. Therefore, the logarithmic mean difference should be used only for low global heat transfer or under limited conditions [17]

$$\overline{h_l} = \frac{\dot{q}_c}{L\Delta T_{lm}} \tag{7}$$

and in the mass transfer coefficient definition:

$$\overline{k_m} = \frac{\dot{m}_{abs}}{L\Delta x_{lm}} \tag{8}$$

where $\Delta T_{lm}$ and $\Delta x_{lm}$ are the logarithmic mean temperature and concentration differences (Eqs. (9) and (10)), respectively; $\dot{q}_c$, $\dot{m}_{abs}$, and $L$ are the heat transferred from the liquid falling film to the cooling fluid, the absorbed mass of the vapor refrigerant into the liquid falling film, and the length of the absorber,

$$\Delta T_{lm} = \frac{(T_{l,i} - T_{c,o}) - (T_{l,o} - T_{c,i})}{\ln\left(\frac{T_{l,i} - T_{c,o}}{T_{l,o} - T_{c,i}}\right)} \tag{9}$$

$$\Delta x_{lm} = \frac{(x_{i,eq} - x_i) - (x_{o,eq} - x_o)}{\ln\left(\frac{x_{i,eq} - x_i}{x_{o,eq} - x_o}\right)} \tag{10}$$

where $T_l$ and $T_c$ are the liquid falling film temperature and the cooling fluid temperature (both $i$-inlet and $o$-outlet), respectively; $x_{eq}$ is the interfacial equilibrium concentration in $T_l$.

Another way to evaluate the heat or mass transfer coefficient is by employing a heat and mass transfer analogy, in which both transport mechanisms are considered merely diffusional through the liquid falling film (e.g. rectification process) and given by Eq. (11) [19], where $M_m$, $Sc$ and $Pr$ are the molecular weight, Schmidt number (0.6–2500) and the Prandtl number (0.6–2500), respectively,

$$\frac{h_l}{k_m} = c_p M_m \left(\frac{Sc}{Pr}\right)^{2/3} \tag{11}$$

Finally, for simultaneous heat and mass transfer processes, Treybal [20] proposed working with a corrected heat transfer coefficient ($h_l^*$), in which the effect of mass transfer on heat transfer are taken into account (Eqs. (12) and (13)). Note that the effect of mass transfer on heat transfer can improve or deteriorate the heat transfer coefficient depending on both process directions, while $\dot{m}_i$ is the mass flow rate for the $i$th component

$$h_l^* = h_l \frac{c}{1 - e^{-c}} \tag{12}$$

$$c = \frac{\dot{m}_A c_{p,A} + \dot{m}_B c_{p,B}}{h_l} \tag{13}$$

Thus, from an experimental work, the link between measured quantities and a relevant definition for transfer coefficients must be established carefully. Consequently, the resulting correlation has to be compared with other studies, as already done in many previous works (see Tables 3 and 6)

## 2.2. Definition of dimensionless numbers, Nu, Sh and Re

Nusselt [21] analyzed the isothermal condensation phenomenon on a flat plate for a pure substance, assuming: laminar regime, Newtonian fluid, constant properties, and without inertial forces from the vapor acting at the interface, obtaining a correlation of the average heat transfer coefficient as a function of the acceleration of gravity, $g$, the Reynolds number, $Re$, and the fluid properties; dynamic viscosity, $\mu$, density, $\rho$, and the liquid thermal conductivity $k$

$$\frac{\overline{h}_l}{k} \left( \frac{\mu_l}{g\rho_l(\rho_l - \rho_v)} \right)^{1/3} = 1.467Re^{-1/3} \tag{14}$$

Neglecting the vapor density ($\rho_v$), and by the definition of kinematic viscosity ($v = \mu/\rho$), Eq. (14) yields,

$$Nu = \frac{\overline{h}_l}{k} \left( \frac{v_l^2}{g} \right)^{1/3} = \frac{\overline{h}_l L_c}{k} = 1.467Re^{-1/3} \tag{15}$$

in which, $L_c = (v^2/g)^{1/3}$ is known as the characteristic length or viscous length scale. However, the Nusselt number ($Nu_\delta$) can be expressed (see e.g. [22,23], as a function of the film thickness, $\delta$, given by:

$$Nu_\delta = \frac{\overline{h}_l \delta}{k} \tag{16}$$

where $\delta$ may be used for the Nusselt film thickness, $\delta_{Nu}$, in which, $\Gamma$ represents the mass flow rate per unit length on each tube side, and $\theta$ the tube angle from the top or the wettability of the tube

$$\delta_{Nu} = \left( \frac{3\mu\Gamma}{g\rho_l(\rho_l - \rho_v)\sin\theta} \right)^{1/3} \cong \left( \frac{3v\Gamma}{\rho_l g \sin\theta} \right)^{1/3} \tag{17}$$

Many correlations are based on $Nu$ (Eq. (15)), while others are based on $Nu_\delta$ (Eq. 16). In order to carry out a comparison between correlations, a common base must be established. Fortunately, both correlations are linked by the following correlation:

$$Nu_\delta = (0.75Re)^{1/3}Nu \tag{18}$$

In the same way, the Sherwood number, $Sh$, is defined as:

$$Sh = \frac{k_m}{D_m} \left( \frac{v^2}{g} \right)^{1/3} \tag{19}$$

and by

$$Sh_\delta = \frac{k_m \delta}{D_m} \tag{20}$$

Thus, the relations are linked by:

$$Sh_\delta = (0.75Re)^{1/3}Sh \tag{21}$$

Analogously, the Reynolds number involves the hydraulic diameter, $D_h$ as the typical length:

$$Re = \frac{\rho V D_h}{\mu} = \frac{4\rho V \delta W}{\mu W} = \frac{4\dot{m}}{\mu W} = \frac{4\Gamma}{\mu} \tag{22}$$

or the typical length can be taken as the film thickness, $\delta$ (see e.g. [2,24,25])

$$Re_\delta = \frac{\rho V \delta}{\mu} \frac{W}{W} = \frac{\dot{m}}{\mu W} = \frac{\Gamma}{\mu} \tag{23}$$

Thus, the relation between these two correlations for the Reynolds number reads:

$$Re = 4Re_\delta \tag{24}$$

where $V$ represents the average fluid velocity, $W$ the width or depth, $\dot{m}$ the mass flow rate. The ratio $\Gamma = \dot{m}/P_{wet}$ between the mass flow and the wet perimeter, is summarized in Table 1,

## 2.3. Classical hypothesis

In order to establish correlations for heat and mass transfer coefficient in sorption processes involving the falling film technology, standard hypotheses are assumed, such as steady-state, incompressible fluid, Newtonian fluid, thermodynamic equilibrium at the liquid-vapor interface, thermal physical properties are constant, non-condensable gases in mixture, and no chemical reactions. However, some additional specific assumptions are commonly encountered in the literature:

- Fluid flow assumptions.
    - Laminar flow regime [2,4,14,22–37].
    - Turbulent flow regime [2].
    - No wave generation at the liquid-vapor interface or smooth falling film. (Waves - known as wavy laminar - improve the heat and mass transfer in the liquid falling film due the transport process. The capillary effects are significant in low Reynolds numbers ($Re \leq 200$), and the inertial effects are relevant in higher Reynolds number ($Re \geqslant 200$) [28]. However, a complete analysis of the simultaneous heat and mass transfer integrated to wave generation onto the interface is complex) [4,22,23,34–36].
    - Wavy flow [28].
    - No interfacial shear or stagnated vapor at constant pressure [2,4,22,23,27,30,31].
    - Shear stress acting at the interface [14,24].
    - Wall friction term is negligible [2,24,26].
    - Vapor and liquid flows are homogeneous [26].
    - No viscous dissipation (in low Reynolds number, this implies low flow velocities and, therefore, viscous dissipation can be neglected) [23,28].
    - No pressure or velocity gradient in the main flow direction [4,14,23].
    - Transport governed by the convective-diffusion [28].
    - 2-D Model [28].
- Thermal transfer assumptions
    - No nucleate flow boiling regime [23,34–36].
    - No heat transfer at the vapor phase [22–24,27,28,30,37].
    - Thermal resistance of tube wall is negligible [22,23,34–36].
    - Heat and mass transfer coefficients constants along the absorber tube [24,26].
    - Vapor pressure driving equal to 0 at the inlet. No thermal entrance effects [2,22,23]. In contrast, Nakoryakov et al. [38] carried out an analysis of these effects in absorption/desorption processes, Cerro and Whitaker did [39] for general transport processes.
    - Cross-streamwise diffusion. No diffusion in the flow direction [22–24,28,30,34].
    - Wall temperature along the tube length changes in a linear fashion [23].
    - Constant wall tube temperature [25,30].
    - No isothermal absorption [2,24].
    - Saturation temperature in the inlet condition [30,32,28].
    - Subcooling temperature in the inlet condition [27,32,40].

## 3. Transfer correlations involving ammonia-water solution

ARC driven by ammonia-water pair can be used in applications of temperature ranging from subzero Celsius degree owing to the ammonia thermodynamic properties. Most studies on transfer correlations in literature focus on the absorber.

## 3.1. Absorber

The most frequent devices involving falling film are horizontal tubes, vertical plate surfaces and helical coil tubes.

### 3.1.1. Horizontal tubes

Bohra [31] carried out an experimental study on an ammonia-water ARC using the falling film technology, in which 24 tubes ($4 \times 6$) of $9.5 \times 10^{-3}$ m OD and 0.29 m length are used. Flow patterns and the transport process are analyzed in his test bench, segmenting the absorber into six distinct parts. The lowest tubes of the array (where the cooling fluid enters in counter-current configuration) obtained higher ammonia absorption rates, similarly to Lee [37] and Lee [41]. In addition, the increase of the solution mass flow rate promoted an upgrade of the heat transfer coefficient because the liquid falling film reached a higher wettability on the tube wall. On the other hand, the heat transfer coefficient decreased as the absorber pressure ($P_{abs}$) and the weak solution concentration ($x_{ws}$) were also decreased. The global heat transfer coefficient ($U$) ranged from 753 to 1853 W m$^{-2}$ °C$^{-1}$, the film heat transfer coefficient ranged ($h_l$) from 923 to 2857 W m$^{-2}$ °C$^{-1}$, the vapor mass transfer coefficient ($k_{m,v}$) ranged from $2.6 \times 10^{-3}$ to 0.25 m s$^{-1}$, and the liquid mass transfer coefficient ($k_{m,l}$) ranged from $5.51 \times 10^{-6}$ to $3.31 \times 10^{-5}$ m s$^{-1}$. The following correlations represent the heat and mass transfer experimentally obtained by Bohra [31], Nusselt number in the segmented liquid falling film, $Nu_{seg,\delta}$

$$Nu_{seg,\delta} = 7.589 \times 10^{-3} Re^{1.04} Pr^{0.45} \left(\frac{P_{abs}}{345}\right)^{-0.145} \tag{25}$$

Sherwood number in the segmented liquid falling film, $Sh_{seg,\delta}$

$$Sh_{seg,\delta} = 1.298 \times 10^{-4} Re^{0.57} Sc^{1.32} \left(\frac{P_{abs}}{345}\right)^{0.644} \tag{26}$$

Lee [37] studied the absorption process in the same test rig as Bohra [31], focusing on the analysis of the overall absorption process, in which both the vapor and the liquid phase correlations are obtained.

Nusselt number in the liquid falling film, $Nu_\delta$

$$Nu_\delta = 3.22 \times 10^{-3} Re^{0.945} Pr^{0.743} \left(\frac{P_{abs}}{345}\right)^{-0.269} \tag{27}$$

Sherwood number in the vapor phase, $Sh_v$

$$Sh_v = 2.708 \times 10^{-11} \left(\frac{Gr_v Sc_v}{Ja_v}\right)^{1.256} \left(\frac{Pr_l}{Sc_l}\right)^{-1.681} \left(\frac{\mu_l - \mu_v}{\mu_v}\right)^{1.426} \tag{28}$$

while $Gr$ and $Ja$ are the Grashof number and the Jakob number, respectively. Sherwood number in liquid falling film, $Sh_\delta$

$$Sh_\delta = 7.437 \times 10^{-4} Re^{0.397} Sc^{1.04} \left(\frac{P_{abs}}{345}\right)^{0.8841} \tag{29}$$

where $P_{abs}$ is given in kPa. Next, Lee et al. [42] carried out an study focused on the absorption rates over horizontal falling film absorbers, using the same test rig and covering the influence of the operational effects over the heat and mass transfer rates. In addition, they compared their results with Wilke's [43], Hu and Jacobi's [44], Kwon and Jeong's [14], and Meacham and Garimella's [45]. Daguenet-Frick et al. [46] used that work to compare the heat transfer coefficient in water vapor absorption in aqueous sodium hydroxide process. However, the Reynolds number was not over the validation range [42].

### 3.1.2. Vertical surface

Kang et al. [27] carried out an experimental work on ammonia-water falling film absorption process using a vertical surface ($110 \times 130 \times 34$ mm$^3$) with offset strip fins (OSF). The simultaneous heat and mass transfer coefficients are analyzed and computed for different operation conditions such as (a) inlet temperatures of the weak liquid solution ($T_{ws} = 17-37.2$ °C) and the ammonia vapor ($T_v = 54.5-66.5$ °C), (b) mass flow rate of weak liquid solution ($\dot{m}_{ws} = 4 \times 10^{-3} - 1 \times 10^{-2}$ kg s$^{-1}$) and the ammonia vapor ($\dot{m}_v = 6.2 \times 10^{-4} - 9 \times 10^{-4}$ kg s$^{-1}$), and (c) weak liquid solution concentration ($x_{ws} = 5$, 10, and 15%). The absorber used water as secondary cooling circuit ($\dot{m}_c = (64.7-79.7) \times 10^{-3}$ kg s$^{-1}$), circulating in a counter flow configuration to the liquid falling film. A rectification process of the wet ammonia vapor was reached before being absorbed by the liquid falling film in the absorption process due to the deeply low level of ammonia vapor purity ($y = 64.7-79.7\%$) and to the inlet subcooling conditions.

The heat and mass transfer ranged from 500 to 2100 W m$^{-2}$ °C$^{-1}$ and from 1.0 to $55 \times 10^{-5}$ m s$^{-1}$, respectively. The increase of the falling film Reynolds number and the mass flow rate of ammonia vapor enhanced the Nusselt and the Sherwood number. However, the Nusselt number was more affected by the liquid mass flow rate than the mass flow of ammonia vapor, while the Sherwood number was more affected by the Reynolds number of ammonia vapor than the Reynolds number of liquid solution. On the other hand, the Sherwood number values were higher than the Nusselt number owing to the Lewis number, meaning that the effective thickness of thermal boundary layer is thicker than that of the diffusion boundary layer [27]. The following Nusselt and Sherwood number correlations are obtained,

Nusselt number in the liquid falling film, $Nu$

$$Nu = 8.530 \times 10^{-2} Re_l^{1.518} Re_v^{0.1759} \left(\frac{T_v - T_l}{T_l}\right)_i^{1.8790} \left(\frac{x_v - x_l}{x_l}\right)_i^{-0.5756} \tag{30}$$

Sherwood number in the liquid falling film, $Sh$

$$Sh = 6.996 \times 10^{-6} Re_l^{0.8874} Re_v^{1.265} \left(\frac{T_v - T_l}{T_l}\right)_i^{0.8844} \left(\frac{x_v - x_l}{x_l}\right)_i^{0.5304} \tag{31}$$

Lee et al. [47] compared the performance of falling film and bubble absorbers for the same operation conditions. Bubble absorbers reached a better performance than falling film for low liquid Reynolds numbers and high vapor Reynolds numbers because there was a partial wettability of the tube in the falling film technology [4]. However, the bubble mode may transfer less heat to the cooling fluid than the falling film for a high liquid solution and low ammonia vapor, resulting in a higher heat generation than of the falling film. Nusselt number in the liquid falling film, $Nu$

$$Nu = 136.9 \times 10^{-4} Re_l^{0.5103} Re_v^{0.02461} \left(\frac{T_v - T_l}{T_l}\right)_i^{0.2977} \left(\frac{x_v - x_l}{x_l}\right)_i^{0.1438} \tag{32}$$

Sherwood number in the liquid falling film, $Sh$

$$Sh = 658.46 Re_l^{0.0195} Re_v^{0.9571} \left(\frac{x_v - x_l}{x_l}\right)_i^{-0.0639} \tag{33}$$

### 3.1.3. Helical coil

The helical geometry may be an alternative to obtain a more compact machine because the heat transfer area per unit volume increases. Jeong et al. [15] experimentally investigated the perfor-

mance of the heat transfer coefficient without mass transport in a coiled tube absorber for various operation conditions such as (a) solution flow rate ($\dot{m}_{ws}$), which was up to $6 \times 10^{-2}$ kg s$^{-1}$, (b) ammonia vapor ($\dot{m}_v$) ranged from $9 \times 10^{-5}$ to $4.2 \times 10^{-4}$ kg s$^{-1}$, and (c) inlet concentration ($x_l$) between 1.2 and 2.2%. The tests were carried out with and without the ammonia absorption process, using a counter-flow absorption in which density ($\rho_l$), temperature ($T$), and pressure ($P$) were used to find the ammonia concentration.

The heat transfer coefficient ($h_l$) was enhanced when the solution flow rate ($\dot{m}_l$) increased (for both with and without absorption process). However, the heat transfer coefficient ($h_l$) associated with the absorption process was lower than the heat transfer obtained for pure water at the same mass flow rate because the ammonia vapor feeding in a counter-flow to the falling film caused an uneven distribution or a stagnation of the liquid falling film [15]. Nevertheless, the mass transfer ($k_m$) behavior was not studied on the test rig. Finally, the Nusselt number as a function only of the Reynolds number was proposed, for ammonia-water

$$Nu = 2.2 \times 10^{-4} Re \quad 50 \leqslant Re \leqslant 300 \tag{34}$$

Kwon and Jeong [14] experimentally analyzed the effect of the vapor flow direction over the heat transfer coefficient ($h_l$) for the absorption process at three different concentrations (3, 14, and 30%) in a helical coil configuration. The effect of the mass flow rate ($\dot{m}_l$) and the temperature of the weak liquid solution ($T_{ws}$) were investigated in the laminar regime ($Re$ = 10–250). A 0.6 m tube length and $12.7 \times 10^{-3}$ m $OD$ was manufactured as a helical coil heat exchanger at $82.7 \times 10^{-3}$ m and $8.0 \times 10^{-2}$ m of an average diameter of a coil (#30) and the header height, respectively. For the balance equations of the absorption process, the heat transferred from the absorber to the cooling fluid circuit was expressed for both absorption processes (heat latent transfer) and change in the solution temperature (sensible heat transfer). The effects of vapor flow over the heat transfer coefficient ($h_l$) were prominent when there was a counter-flow absorption and a low ammonia concentration (3%) because, in small concentrations, the vapor has high specific volume. Moreover, the liquid falling film flow pattern may be affected by a high velocity of the vapor flow. The Nusselt number was higher in the co-current absorption than in the counter-flow absorption. However, at a higher ammonia concentration (30%), the behavior of the Nusselt number was similar for both co-current and counter-flow absorption processes. In addition, the increase in the liquid solution mass flow rate improved the heat transfer coefficient. On the other hand, the effect of the weak liquid solution temperature over the heat transfer was negligible when it was compared with other operational parameters.

The Nusselt number for the liquid falling film for co-current absorption is given by Eq. (35), where $\tau_v^*$ is a non-dimensional shear stress detailed by Kwon and Jeong [14],

$$Nu = 1.975 \times 10^{-3} Re_l^{0.6895} \tau_v^{*-0.0249} \tag{35}$$

Nusselt number in the liquid falling film for counter-current absorption

$$Nu = 1.683 \times 10^{-4} Re_l^{0.8672} \tau_v^{*-0.3018} \tag{36}$$

### 3.2. Generator using horizontal tubes

Zavaleta-Aguilar and Simões-Moreira [36] analyzed a falling film generator (distiller) to optimize the concentration ($y$) and the mass flow rate of distilled ($\dot{m}_y$) when the ammonia vapor is separated from the ammonia-water solution, researching some mean parameters such as strong solution concentration ($x_{ss}$),

strong solution mass flow rate ($\dot{m}_{ss}$), rectifier temperature ($T_{rect}$), wall temperature ($T_w$) and strong solution temperature of inlet ($T_{ss}$). A horizontal tube bundle geometry was used as a generator and rectifier, analyzing the hydraulic behavior of the liquid film and the distillation degree of purity. In the first one, a total wettability on the tubes was reached due to the small intertube distance, ($S - D = 2$ mm), homogeneous liquid distribution, and a superficial treatment by sand blasting over the wall tube.

A distilled ammonia concentration ($y$) up to 99.74% was obtained for an ammonia-water concentration of $x_{ss} = 49\%$. In addition, the purity of distilled ammonia ($y$) was enhanced when the strong solution mass flow ($\dot{m}_{ss}$) and the strong solution concentration ($x_{ss}$) were increased, or when the average rectifier temperature ($T_{rect}$), wall temperature ($T_w$) in the generator, and the strong solution temperature ($T_{ss}$) were reduced. The experimental work was carried out for a strong solution mass flow of $1.6 \times 10^{-2}$ to $2.76 \times 10^{-2}$ kg s$^{-1}$ equivalent to Reynolds numbers of 108–246. They employed two ammonia concentrations (0.37 and 0.49). The concentration of ammonia distilled ($y$) was increased, and the distilled mass flow rate ($\dot{m}_y$) was diminished with the increase of the mass flow rate ($\dot{m}_{ss}$) when the wall temperature and the rectifier temperature were kept constant, because the heat transfer coefficient diminishes due to the thickening of the liquid film, increasing the thermal resistance throughout the liquid film. According to the rectifier temperature, higher ammonia distilled concentration was obtained at the cooler temperatures since it rejected more water of the wet ammonia vapor [36].

Regarding the wall temperature ($T_w$), the distilled mass flow ($\dot{m}_y$) improved for the highest wall temperature ($T_w$) in the generator, however, the distilled concentration diminished ($y$), because a higher wall temperature promoted the evaporation of more wet vapor [36]. The following correlation was derived for the heat transfer on the liquid film:

$$Nu = 0.75 Re^{-0.27} Pr^{0.4} \tag{37}$$

### 3.3. Summary of transfer correlations

In this section, the correlations presented previously are summarized. In Table 2, the application range of properties and dimensionless numbers applied to ammonia-water solution is summarized. Most of the correlations are devoted to the absorption machine. To our knowledge, there exists only one work in the open literature proposing a correlation for a generator using ammonia-water solution [36]. The first and second column shows the authors and their correlations, respectively; Next, Prandtl, Reynolds, and Schmidt numbers are showed; while temperature and pressure of application are shown in next two columns. The two last columns present the concentration of the liquid solution ($x$) and the vapor ($y$), and the remarks for each correlation. Finally, in Table 3, configurations of the experimental set up are summarized. The first column presents the author, the second column shows geometrical configurations; next column associates other studies that they have been used for comparing. Finally, some comments was carried out in last column.

## 4. Transfer correlations involving lithium bromide-water solution

The sorption machine using lithium bromide solution works both at *low* pressure (around 1 $kPa$) where the $Li - Br$ solution absorbers the water vapor, and at *high* pressure (around 10 $kPa$) where the desorption process occurs. Although the absorber constitutes the critical device in the machine, many studies have also focused on the generator.

## 4.1. Generator

The main devices used for generators involving lithium-bromide pair are vertical tubes and horizontal tubes.

### 4.1.1. Vertical tubes

Shi et al. [34] carried out a mathematical simulation and experimental work of a desorption process inside a vertical tube of 25 mm OD and 760 mm in length, analyzing the influence of the heat flux and the volume flow rate over the heat transfer coefficient for a single absorption pressure (97.25 kPa), solution concentration of 49.5%, heat flux ranging 5–25 kW m$^{-2}$, and for Reynolds smaller than 500.[1] In the mathematical analysis, the interfacial effects, wave generation in the liquid film, changes in film thickness, and pool boiling by superheating (only by the evaporation on the interface) were neglected. In addition, the performance of the flooded generator and the falling film evaporator were compared for the same heat flux. The heat transfer coefficient (1000−1800 W m$^{-2}$ °C$^{-1}$) was enhanced when the heat flux was increased for different volume flow solutions. However, the heat transfer rate decreased with the increases of the volume flow solution when the Reynolds number was less than $Re_\delta \leq 500$ or $Re \leq 2000$, and for $Re_\delta \geqslant 500$. The heat transfer behavior was the opposite when the volume flow was incremented because there was a regime transition from the laminar to the turbulent regime.

According to the numerical and experimental analysis, both results of the heat transfer coefficient were compared, having the heat transfer coefficient underestimated by the numerical study due to the simplified hypotheses previously mentioned. Finally, the falling film evaporator had the best performance of the heat transfer coefficient for heat flux lower than 12.000 W m$^{-2}$ as compared with the flooded generator.

Heat transfer coefficient (±19% maximum deviation) for the liquid-phase

$$h_l = 14 \times 10^3 q_w''^{0.0764} Re_l^{-0.5391} \tag{38}$$

Later, Shi et al. [35] built a test rig to investigate the heat transfer behavior for a vertical in-tube falling film generator, testing different heat fluxes (10−25 kW m$^{-2}$) and concentrations of lithium bromide (49.5−58%) for a laminar regime ($Re = 287−770$), and for other operation conditions such as (a) generation pressure of 9.725 kPa and (b) volume flow rate range of 7−14 ml s$^{-1}$. A 25 mm O.D stainless steel tube and 760 mm length was employed, in which the lithium bromide solution was fed inside the tube top in the saturated condition. In addition, the falling film technology was compared with the flooded generator as well.

According to the inlet concentration of lithium bromide solution, the change in this parameter promoted the variation in the thermophysical properties, meaning the increases of the viscosity and the surface tension when the concentration was increased, diminishing the inertial flow effects, and thus, the convection heat transfer decrease on the solution side. On the other hand, the increase of the heat flux may have modified the heat transfer mechanism from the evaporation process given at the interface to the evaporation process accompanied by nucleate boiling, which implied increase of the heat transfer coefficient, as usual. However, Shi et al. [35] did not study these phenomena in an independent fashion. Finally, the heat transfer coefficient in the falling film technology reached higher performance (up to 4 times) than flooded tube generator, making the design of a desorption equipment more compact. Heat transfer coefficient for the liquid-phase

$$h_l = 129.7712 x_i^{-0.8058} q_w^{0.2422} Re_l^{-0.0856} \tag{39}$$

---

[1] Reynolds number was defined as a function of the film thickness, $Re_\delta$.

where $x_i$ is the weak solution concentration at the inlet condition and $q_w$ is the heat transferred by the wall.

### 4.1.2. Horizontal tubes

Jani et al. [30] developed a model to analytically study the heat and mass transfer coefficient in a falling film generator over a horizontal tube bundle, in which the Reynolds numbers (in the laminar regime without wave generation), tube diameter, tube spacing, and thermophysical properties were analyzed. The model took into account three regions over the horizontal tubes for different heat and mass transfer phenomena, being (a) impingement region on the top of the tubes, (b) vertical liquid sheet for the tube spacing, and (c) tube bundle for all horizontal tubes. Prandtl numbers ranged from 7 to 10, Reynolds number ranged from 100 to 500, generation pressure from 5 to 10 kPa, and lithium bromide concentration from 50 to 60%.

The average heat transfer coefficient decreased with the increase of the number of tubes in the vertical position in the bundle tube, being expressed as a function of the tube numbers ($N$) and the heat transfer coefficient ($h$) of the first tube, $hN^{-0.25}$. For low Reynolds numbers ($Re \leq 200$), the increase in the Reynolds number improved the average heat transfer rate. However, above this value, the effects of the Reynolds number over the average heat transfer coefficient may be neglected as well as the generation pressure variations or the superheating wall.

Nusselt number for the liquid phase for one tube

$$Nu = 54.41 \times 10^{-2} Re_l^{0.1597} Pr_l^{0.4563} D^{*-0.3971} s^{*0.001626} P^{0.0213} e^{-0.004598X} \tag{40}$$

Nusselt number for bundle tube

$$Nu = 54.41 \times 10^{-2} Re_l^{0.1597} Pr_l^{0.4563} D^{*-0.3971} s^{*0.001626} P^{0.0213}$$
$$\times e^{-0.004598X} \cdot N^{-0.25} \tag{41}$$

where $D^*$ and $s^*$ represent the dimensionless tube diameter ($D/L_c$) and the dimensionless vertical tube spacing ($s/L_c$), respectively. $L_c$ represents the characteristic length $(v^2/g)^{1/3}$.

Jani [57] proposed correlations for the dimensionless heat and mass transfer coefficients obtained by numerical modeling. The configuration studied corresponds to a solution of $Li − Br$ falling down over a horizontal single heated tube.

The model used for the hydrodynamic part corresponds to the Nusselt solution (the stream-wise component of velocity is quadratic for a given cross section of the liquid film) but varied following the angle along the tube. The transport equations correspond to the steady advection-diffusion equations. An increase of absorption pressure led to an increment of the saturation temperature of the solution, reducing the viscosity of solution, and therefore, an enhancement of the heat and mass transfer coefficient. On the other hand, the viscosity could be increased with a higher inlet concentration, negatively affecting the equipment performance [57]. The correlations obtained were Nusselt number for the liquid phase

$$Nu = 78.93 \times 10^{-2} Re_l^{0.16587} Pr_l^{0.37275} Sc_l^{-0.041769} D^{*-0.40335} \tag{42}$$

Sherwood number for the liquid phase

$$Sh = 2 \times 10^{-3} \times Re_l^{1.0023} Pr_l^{-0.74049} Sc_l^{1.3455} D^{*-1.0006} \tag{43}$$

where $D^*$ represents the dimensionless diameter of the tube as previously defined. The range of validity holds for values of $Pr$ between 7 and 10, values of $Re$ between 100 and 500. The pressure values from 5 kPa to 10 kPa and the concentration of lithium bromide used was around 50–60%

According to the results, the $Nu$ number increased as the $Re_l$ number also increased, but seemed to be unaffected by the $Sc_l$

number. The $Sh$ number grew linearly with the $Re_l$ number but remained proportionally inverse to the tube diameter. An increase of the generator pressure (or saturation temperature) and/or a reduction of the inlet concentration improved the heat transfer coefficient due to the thinning of the falling film by a decrease of the viscosity.

## 4.2. Absorber

Most of the works devoted to absorbers using lithium bromide-water solution are focused on vertical flat plate and horizontal tubes.

### 4.2.1. Flat plate

Kim and Ferreira [32] studied the heat and mass transfer coefficients enhancement, for vertical plate absorber, thanks to the presence of wire screen, when the $Re_l$ number is varying (from 40 to 110). In their investigation, four different liquid films are used: pure water and a 50% Li − Br solution, with or without 100 ppm of 2-ethyl-1-hexanol (2-EH) as additive. The experimental setup uses a flat copper plate that may be covered by a wire screen. For the whole 39 data set obtained, the range used for pressure was from 0.7 to 2.9 kPa. The mass flow rate at the inlet varied from $0.6 \times 10^{-3}$ to $7.7 \times 10^{-3}$ kg s$^{-1}$.

The resulting correlations are given by: Nusselt number for the liquid phase

$$Nu = a \times Re_l^b Pr_l^{0.5} \tag{44}$$

Sherwood number for the liquid phase

$$Sh = c \times Re_l^d Sc_l^{0.5} \tag{45}$$

where, for 4 configurations (over the 10 performed), the coefficients are presented in Table 4.

The global result shows that the presence of the wire screen tends to decrease both heat and mass transfer coefficients of Li − Br solution when mixed with the 2-EH additive. Specifically, for the heat transfer coefficient, the screened surface slightly enhances transfers by promoting the wetting surface of pure Li-Br solution, in comparison with the bare surface. Yet the reciprocal occurs when 2-EH is added: the screen tends to reduce the heat transfer. For the mass transfer, the $Sh$ number remains higher when the solution is water-cooled than for the adiabatic case. In the former configuration, the presence of the wire screen tends to weaken the mass diffusion when the 2-EH additive is used. The wire screen produces the converse effect (increasing the mass diffusion) for solutions without additive. The presence of the wire screen seems not to produce any significant effect on the $Sh$ number for other configurations.

However, the authors highlight that their analysis does not take into account incomplete wetting. Moreover, an error analysis yielding a possible error to heat transfer coefficient estimation of ±20%, in case of water-cooled absorption.

Karami and Farhanieh [22] carried out a numerical study of the simultaneous heat and mass transfer phenomenon in the absorption process in a vertical plate using the lithium bromide-water as the working fluid, analyzing (a) the effects of the solution mass flow ($Re = 5-150$), (b) inlet cooling temperature, and (c) the inlet solution concentration. A fully implicit finite-difference method was used to solve the one-dimensional mass, energy and momentum equations, analyzing the grid size effects and then employed the $800 \times 160$ mesh, and the mass flux value as convergence criteria ($10^{-6}$). The temperature distribution across the film thickness was assumed to be linear due to the dominating heat only conduction effect, in which the lowest temperature profile was obtained in the last section of the absorber. The mass transfer rate reached

a maximum value of $51.80 \times 10^{-4}$ kg m$^{-2}$ s. The local heat transfer coefficient changed as a function of the vertical position on the plate (up to 5 times). Nevertheless, the local mass transfer coefficient was strongly dependent on the vertical position (up to 12 times), having the highest values in the first section of the absorber [22]. The correlations based on the numerical results were, Nusselt number for the liquid phase

$$Nu_\delta = 47.67 \times 10^{-2} Re_l^{0.0477} Pr_l^{0.334} \tag{46}$$

Sherwood number for the liquid phase

$$Sh_\delta = 13.29 \times 10^{-2} Re_l^{1.0571} Sc_l^{0.334} \tag{47}$$

Later, Karami and Farhanieh [23] carried out the similar numerical modeling to analyze the simultaneous heat and mass transfer behavior for different inclinations of the flat plate, covering from the quasi-horizontal position ($\beta = 10°$) up to the vertical position ($\beta = 90°$). The absorption mechanism occurring within the film was modeled by the 2D steady advection-diffusion equations, tested for the absorption pressure of $P = 1$ kPa, inlet solution temperature fixed at 45 °C, whereas the inlet concentration was 60%. The properties of the lithium bromide-water solution were taken from McNeely [58].The Reynolds number ranged from 4 up to 150 for different flat plate inclinations, $\beta$, proposing the following correlations, Nusselt heat transfer for the liquid phase

$$Nu_\delta = A \cdot Re_l^B Pr_l^{0.334} \tag{48}$$

Sherwood number for the liquid phase

$$Sh_\delta = C \cdot Re_l^D Sc_l^{0.334} \tag{49}$$

with coefficients $A$, $B$, $C$ and $D$ depending on the angle and given by Eqs. (50)–(53).

$$A = 6 \times 10^{-8} \beta^3 - 2 \times 10^{-5} \beta^2 + 1.4 \times 10^{-3} \beta + 1.58 \times 10^{-2} \tag{50}$$
$$B = -1 \times 10^{-7} \beta^3 + 3 \times 10^{-5} \beta^2 - 3 \times 10^{-3} \beta + 5.637 \times 10^{-1} \tag{51}$$
$$C = -2 \times 10^{-7} \beta^3 + 3 \times 10^{-5} \beta^2 - 2.3 \times 10^{-3} \beta + 1.31 \times 10^{-1} \tag{52}$$
$$D = 3.23 \times 10^{-6} \beta^2 - 6.19 \times 10^{-4} \beta + 1.16 \tag{53}$$

Following their results, the averaged $Nu$ does not seem to be highly affected (variations inferior to 0.07) for different inclination at $Re_l = 20.5$, whereas the averaged $Sh$ number reduces by about 42% (from 46 to 27) when the angle goes from 10° to 90°. Moreover, the formulas performed shows that the optimal angle for the averaged $Nu$ seems to be for an inclination around $\beta = 85°$.

### 4.2.2. Horizontal tubes

Babadi and Farhanieh [59] developed an analytical study of the heat and mass transfer phenomena in the lithium bromide-water absorption process over a horizontal tube for operation conditions such as (a) Reynolds number ranging from 5 to 100, (b) absorption pressure of 1 kPa, (c) inlet concentration of 62%, (d) wall temperature of 32 °C, and (e) inlet temperature of 40 °C. The average heat transfer coefficient ranged between 2000 and 5000 W m$^{-2}$ °C$^{-1}$. A large temperature difference between the tube wall and the inlet solution promoted the highest value of heat transfer rate. In contrast, at the outlet region, the heat transfer decreased due to the thickening of the liquid film, increasing the thermal resistance. Moreover, the film thickness was associated with the Reynolds number changes, meaning the diminishing of the heat transfer rate with the decreasing of the Reynolds number due to the viscosity effects were more prominent than the inertial effects. In the opposite behavior, a high Reynolds number promoted convective heat transfer rate. Nevertheless, the Reynolds number influence was more dominant over the mass transfer than over the heat transfer

rate [59]. Banasiak and Kozioł [60] used this study to compute the heat transfer coefficient,

Nusselt number for the liquid phase

$$Nu = 0.45Re_l^{-0.23}Pr_l^{0.33} \quad \text{for} \quad Re < 60 \tag{54}$$

Sherwood number for the liquid phase

$$Sh = 1.03Re_l^{-0.146}\left(\frac{Sc_l}{1000}\right)^{1.42} \quad \text{for} \quad Re < \left(\frac{Sc_l}{5367}\right)^{-3.61} \tag{55}$$

$$Sh = 9.4 \times 10^{-2}Re_l^{0.29}\left(\frac{Sc_l}{1000}\right)^{2.6} \quad \text{for} \quad Re > \left(\frac{Sc_l}{5367}\right)^{-3.61} \tag{56}$$

### 4.3. Summary of transfer correlations

Tables 5 and 6.

## 5. Other works devoted to transfer coefficient study

Some other works focus on establishing a formula for heat transfer coefficient. These works may involve the specific geometric length (whose influence has been suggested in the previous graphs), or the study is simply dedicated to fluid couples other than ammonia-water or lithium bromide-water.

### 5.1. Works using lithium bromide-water couple

Yüksel and Schlünder [2] carried out an experimental study of a non isothermal absorption in liquid films for the laminar and turbulent regime, in which the local and the average heat and mass transfer coefficients were analyzed. A vertical tube with variable length (0–2.5 m) and the counter-current absorption was configured. There was not any mass transfer resistance in the vapor phase and the film surface temperature was measured by infrared pyrometer (±0.3 K).Two partial heat transfer coefficients were defined, being (a) from the film surface to the bulk, and (b) from the bulk to the vapor-liquid interface. For the former, the wall temperature and the bulk temperature were taken into account, and for the second, the bulk temperature and the interface were taken into account (Eqs. (2) and (3)). The average heat and mass transfer were given by,

$$\bar{h}_l = \frac{\dot{m}''_{abs}\Delta i_{abs}}{T_{int} - T_w} \tag{57}$$

$$\bar{k}_m = \frac{\dot{m}''_{abs}}{\pi D\bar{\rho}_l \int_0^L \ln\left(\frac{1-x_b(L)}{1-x_{int}(L)}\right)} \tag{58}$$

For the turbulent regime, it was assumed that the interface temperature has the same value as the bulk temperature, and the turbulence is damped in the vicinity of the vapor-liquid interface due to surface tension effects; thus, at the interface, the heat, mass and momentum transfer were only possible by molecular transfer, making possible to use an analogy between the temperature and concentration profile (Nu/Sh) as follows [2];

$$\left(\frac{1-x_b}{1-x_{int}(T_{int},P)}\right)^{\frac{c_{p,water}}{c_{p,l}}\frac{1}{Le^{1-n}}} = \frac{c_{p,water}}{\Delta i_{abs}}(T_{int} - T_b) + 1 \tag{59}$$

The values for n are between 0.4 and 0.5 for isothermal falling film absorption. They found that assuming the same value for the bulk and the interface temperatures led to low Sherwood numbers. However, their results of mass transfer obtained by interface temperature measurements agreed well with the calculated by Nu/Sh

analogy. In addition, for the Reynolds number in the 100–500 range, the mass transfer is highly sensitive to the vapor phase velocity because it amplified the shear stress over the interface. The turbulent regime is less dependent on this condition because the mass transport is severe in the turbulence [2]. According to the Nusselt number, the Nu/Sh analogy agrees with that computed by interface temperature measurements, but when it take into account the assumption of the same temperature between bulk and interface, it overestimates the Nusselt number.

Yüksel and Schlünder [24] carried out a mathematical modeling of turbulent heat and mass transfer in a non-isothermal falling film absorption, in which the mean assumptions were taken into account: (a) the transversal velocity does not influence the momentum transfer, (b) no axial diffusive transport process, (c) no pressure gradients into the film, (d) shear stress acting on a differential element of the film, (e) film thickness computed by continuity equation, (f) eddy viscosity into the film determines the velocity distribution into the film, (g) unidirectional mass transfer, and (h) equilibrium condition at the interface. According to the profile of the eddy transport coefficients, it investigated several proposals, but it was found that most of the authors employed the van Driest [71] equation for calculating the eddy viscosity profile near the wall tube. However, near the interface, the authors supposed damped turbulence, in which the mass transport takes place only near the interface [24]. Regarding to the Nusselt number, the numerical results that were computed using various eddy transport coefficients were higher than the experimental results in Yüksel and Schlünder [2], however, the numerical mass transfer coefficient agreed well with the experimental study because the assumption of the turbulence model that considered the damping effect (near the wall and near the interface) was suitable. In addition, they suggested a new dimensionless group to describe the effect of the thermophysical properties in the Nusselt number.

Patnaik and Perez-Blanco [28] investigated the simultaneous heat and mass transfer in the absorption process for the wavy film flow, employing an iterative finite-difference method for a transient and two-dimensional (2-D) model, testing the operation conditions such as (a) inlet concentration of 60%, (b) absorption pressure of 0.850 kPa, (c) inlet temperature solution of 40 °C, (d) surface temperature of 35 °C, and (e) wavy-laminar regime 200 ⩽ Re ⩽ 1000, in which there are two types of wavy laminar. The mass transfer rate was found to be higher in wavy laminar than in smooth laminar regime due to the inertial and roll waves it promotes, enhancing the normal convective flux

$$Nu = \delta Re_l Pr_l\left[(T_i - T_o) + \left(\frac{x_i - x_o}{x_o}\right)\frac{i_{abs}}{c_{p,l}}\right](4L\Delta T_{lm})^{-1} \tag{60}$$

$$Sh = \delta Re_l Sc_l((x_i - x_o))(4Lx_o\Delta x_{lm})^{-1} \tag{61}$$

Takamatsu et al. [29] studied the heat and mass transfer behavior in a 400 mm long falling vertical in-tube absorber, comparing the results with the previously reported 1200mmlong, in which the effect of the solution flow rate ($13 \times 10^{-3} - 25 \times 10^{-3}$ kg s$^{-1}$), solution subcooling temperature ($\Delta T_{sub} = 0$ °C and $\Delta T_{sub} = 5$ °C), and cooling water temperature ($T_{l,i} = 34$; 35 °C) were tested. The experimental work found the total wettability of the tube when the Reynolds number reached Re = 130. Nevertheless, the film break-down may happen below this value, causing the deterioration of the average heat and mass transfer coefficient. In addition, it pointed out that the logarithmic mean difference in concentration is not always valid for the absorber, diverging from the real driving force of the absorption process. According to the absorption process, when the solution was fed at the saturated condition ($\Delta T_{sub} = 0$ °C), the absorption process started after the thermal boundary layer on the cooled wall reaching the vapor-liquid inter-

face, and for the subcooled condition, the absorption process began in the inlet of the absorber. The higher absorption process was given at the first 0.4 m (15–50%) when compared with the last 0.8 m section, explained due to the wettability problems, such as the breaking film. This allows concluding that the absorption process was deeply influenced by the tube length [29].

## 5.2. Works involving falling film technology

- Nosoko et al. [25] carried out an experimental study of oxygen gas absorption in falling water films over horizontal tubes in the laminar regime (10–150). There was a complete tube wettability without additives, using copper tubes and a capillary tube of distribution. It tested various tube spacings $(2 - 15) \times 10^{-3}$ m and flow rates, in which an isothermal film was assumed due to the low heat of absorption of the oxygen. The logarithmic mean concentration difference and the equilibrium condition at the interface were used to calculate the mass transfer coefficient, in which all the tests were developed in atmospheric pressure, and the temperature ranged between 18 and 23 °C. It was concluded that the droplet flow promotes more increase of the mass transfer than the sheet droplet because it penetrates the film depth, enhancing the mass transfer coefficient at the wall-film interface, and the mass transfer could improve up to 45%, on the Reynolds number 30–150. On the other hand, the Sherwood number improved when the tube spacing increased from $2 \times 10^{-3}$ to $5 \times 10^{-3}$ m, and it was kept constant for higher tube spacing, such as higher than 10 [25]. The following correlations were obtained:

$$Sh = 37.77 \times 10^{-3}Re_l^{0.86}Sc_l^{0.5} \tag{62}$$

- Goel and Goswami [72,73], and Triché et al. [74] used the Wilke correlation [43] to compute the heat transfer coefficient for the laminar flow regime, in which Wilke [43] studied the falling film heat transfer, and Kandlikar [75] showed the next follows, For $Re \leqslant 2460Pr^{-0.646}$

$$Nu = 1.92Re^{-1/3} \tag{63}$$

For $2460Pr^{-0.646} \leqslant Re \leqslant 1600$

$$Nu = 32.3 \times 10^{-3}Re^{1/5}Pr^{0.344} \tag{64}$$

For $1600 \leqslant Re \leqslant 3200$

$$Nu = 10.2 \times 10^{-4}Re^{2/3}Pr^{0.344} \tag{65}$$

For $3200 \leqslant Re$

$$Nu = 8.7 \times 10^{-3}Re^{2/5}Pr^{0.344} \tag{66}$$

- Chun and Seban [52,76] is given by; Laminar regime, $Re \leqslant 2.44Ka^{-1/11}$ is given by:

$$Nu = 0.822Re^{-1/3} \tag{67}$$

Wavy laminar regime, $2.44Ka^{-1/11} \leqslant Re \leqslant 5800Pr^{-1.06}$

$$Nu = 0.822Re^{-0.22} \tag{68}$$

Turbulent regime, and the departure from the wavy laminar to turbulent regime $Re = 5800Pr^{-1.06}$

$$Nu = 3.8 \times 10^{-3}Re^{0.4}Pr^{0.65} \tag{69}$$

- Hu and Jacobi [44], sheet mode

$$Nu = 2.194Re^{0.28}Pr^{0.14}Ar^{-0.20}\left(\frac{S-D}{D}\right)^{0.07} \tag{70}$$

Jet mode, and the departure from the jet mode to the sheet mode is $Re = 1.431Ga^{0.234}$.

$$Nu = 1.378Re^{0.242}Pr^{0.26}Ar^{-0.23}\left(\frac{S-D}{D}\right)^{0.08} \tag{71}$$

Droplet mode, and the departure from the droplet mode to the jet is $Re = 8.4 \times 10^{-2}Ga^{0.302}$.

$$Nu = 0.113Re^{0.85}Pr^{0.85}Ar^{-0.27}\left(\frac{S-D}{D}\right)^{0.04} \tag{72}$$

- Alhusseini et al. [77], laminar regime

$$Nu = 2.65Re^{-0.158}Ka^{0.0563} \tag{73}$$

and turbulent regime,

$$Nu = \frac{Pr\delta^{*1/3}}{A_1Pr^{3/4} + A_2Pr^{1/2} + A_3Pr^{1/4} + C_1 + B_1Ka^{1/2}Pr^{1/2}} \tag{74}$$

where
- $A_1 = 9.17$;
- $A_2 = 0.328\pi(130 + \delta^*)$;
- $A_3 = 0.289(152100 + 2340\delta^* + 7\delta^{*2})/\delta^{*2}$;
- $B_1 = (2.51x10^6\delta^{*1/3}Ka^{-0.173})/Re^{(3.49Ka^{0.0675})}$;
- $C_1 = 8.82 + 3 \times 10^{-4}Re$;
- $\delta^* = 94.6 \times 10^{-3}Re^{0.8}$;
- Shahzada et al. [78] modified the Han and Flecter's correlation, getting;

$$Nu = 1.7 \times 10^{-3}\left(\frac{v^2}{gk^3}\right)^{-0.276}Re^{-1/3}Pr^{-0.75}\left[2e^{S/S_o} - 1\right]^{0.07}\left(\frac{T_{sat}}{322}\right)^{0.73} \tag{75}$$

and the modified of Chun and Seban's correlation [52], getting;

$$Nu = 0.20\left(\frac{v^2}{gk^3}\right)^{0.23}Re^{1.66}\left[2e^{S/S_o} - 1\right]^{0.006}\left(\frac{T_{sat}}{319}\right)^{-1.01} \tag{76}$$

where, $S_o = 3 \times 10^4$ ppm, while $S$ is the salt concentration given in ppm, $T_{sat}$ is the saturation temperature given in $K$.

- Parken et al. [79], for the $25.4 \times 10^{-3}$ m diameter tube

$$Nu = 4.2 \times 10^{-2}Re^{0.15}Pr^{0.53} \tag{77}$$

for the 50.8 mm diameter tube

$$Nu = 3.8 \times 10^{-2}Re^{0.15}Pr^{0.53} \tag{78}$$

- Mitrovic [53], for $160 \leqslant Re \leqslant 560$

$$Nu = 13.74 \times 10^{-2}Re^{0.349}Pr^{0.5}\beta \tag{79}$$

where, $\beta = \frac{(S/D)^{0.158}}{1 + e^{0.008Re^{1.32}}}$

- Liu et al. [80] for $1.75 \leqslant Pr \leqslant 7.02$; $800 \leqslant Re \leqslant 5000$; $213 \leqslant Ar \leqslant 1546$; $1 \times 10^4 m \leqslant D \leqslant 4 \times 10^4$ m,

$$Nu = 4.1 \times 10^{-2}Re^{0.3}Pr^{0.66}Ar^{-0.12} \tag{80}$$

- Chien [81] for R-245fa, $6.26 \leqslant Pr \leqslant 7.15$; $115 \leqslant Re \leqslant 372$; $16.5 \times 10^{-5} \leqslant We \leqslant 16.8 \times 10^{-5}$,

$$Nu = 38.6 \times 10^{-3}Re^{0.09}Pr^{0.986} \tag{81}$$

- Narváez-Romo and Simões-Moreira [82] for water, $0.72 \leqslant Pr \leqslant 7.92$; $160 \leqslant Re \leqslant 940$,

$$Nu = 0.21Re^{-0.067}Pr^{0.528} \tag{82}$$

- Leite [83] developed a numerical study of both absorber and generator, applying the finite difference method for an inclined plate, in which the mass, species and energy balances were employed. Both components were modeled for various operation conditions, testing the geometry dimensions, plate angle of inclination, wall temperature and the inlet conditions. The

results confirmed that the vertical position is the best position of performance, promoting a stable operation condition. Finally a correlation between the heat and mass transfer over an inclined plate as a function of the vertical position is obtained by:

$$F_{Nu}(\beta) = \frac{Nu(\beta)}{Nu(\pi/2)} \tag{83}$$

$$F_{Sh}(\beta) = \frac{Sh(\beta)}{Sh(\pi/2)} \tag{84}$$

$$F_{Nu}(\beta) = e^{-0.081(\beta-\pi/2)+0.054(\beta^2-\pi^2/4)-0.012(\beta^3-\pi^3/8)} \tag{85}$$

$$F_{Sh}(\beta) = e^{-1.712(\beta-\pi/2)+1.402(\beta^2-\pi^2/4)-0.392(\beta^3-\pi^3/8)} \tag{86}$$

These factors were obtained by fitting the numerical results of Karami and Farhanieh [23]. In addition, the correlation of Kang et al. [27] was used to compute the heat and mass transfer coefficient for the vertical position ($\beta = \pi/2$).

Next, an analysis of the heat and mass transfer behavior is carried out, in which all previous correlations (Nusselt and Sherwood numbers) are evaluated and compared to each other based on the typical operational conditions of an ARC, obtaining a possible heat and mass transfer mapping for refrigeration ($T = 253$) and air-conditioning ($T = 280$) applications. Next Section aims to obtain a fair comparison of correlations in the framework of the simulation of a realistic ARC, allowing integrate the correlations with operating conditions of ARCs.

## 6. Heat and mass transfer mapping for refrigeration and air-conditioning applications

This section presents analyses of previous correlations that can be applied directly to ammonia-water and lithium bromide-water ARCs at typical operational conditions.

### 6.1. Ammonia-water working fluid pair

Table 7 shows some typical operation conditions for an ARC, in which eight operation conditions are evaluated and shown in the first column. The second, third, and fourth column show the condensation temperature ($T_{con}$), vaporization temperature ($T_{eva}$) and generation temperature $T_{gen}$, respectively; while, COP, $P_{abs}$ and $P_{gen}$ are the coefficient of performance, absorption pressure and generation pressure, respectively; Next, $x_{ss}$, $x_{ws}$ are the strong and weak solution concentrations, respectively; Finally, the last two columns show the Prandtl number (Pr) and Schmidt number (Sc) for the given absorption conditions.

Fig. 3 shows the Sherwood number, which shows that the mass transfer is enhanced as the Reynolds number is
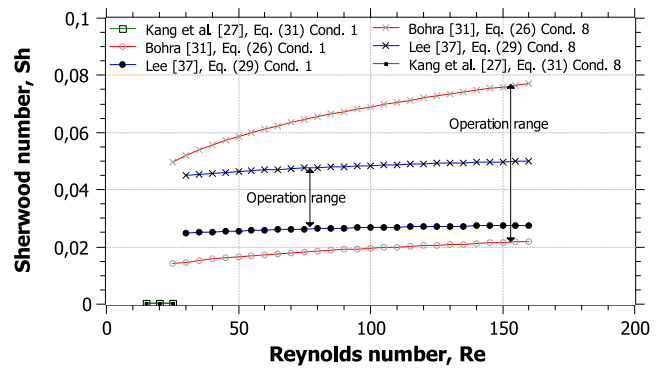


**Fig. 3.** Sherwood number as a function of the Reynolds number for the ammonia-water solution.

increased.Also, the mass transfer coefficient strongly increases as the absorption refrigeration cycle achieves vaporization temperatures below 0 °C. Moreover, Fig. 3 displays the possible mass transfer mapping for the ARC for the whole operational conditions given in Tables 2 and 7. The mass transfer mapping from Bohra [31] agrees with Lee's [37]. However, Kang et al.'s correlation [27] underestimates these values, in which it may be explained by the conditions that the experiments are carried out at the test rig (low purity of ammonia vapor). Therefore, the Sherwood number may vary from 0.015 to 0.08 for the Reynolds number ranging from 10 to 150 in $NH_3 - H_2O$ ARC in refrigeration and air conditioning applications. The operational conditions 2–7 are not shown in Fig. 3, but these values are found within of these ranges.

Fig. 4 shows the Nusselt number as a function of the Reynolds number. Fig. 4a displays the correlations used in the falling film technology using ammonia-water and other working fluids for an evaporation process, in which these correlations such as those proposed by Zavaleta-Aguilar and Simões-Moreira[36], Wilke [43], Chun and Seban [52], Alhusseini et al. [77], and Narváez-Romo and Simões-Moreira [82] show similar heat transfer values from Bohra's [31] data (absorption process) for the Reynolds numbers between 100 and 150. However, the trend of these processes are in opposition to each other. Fig. 4b displays a comparison between the correlations of Kwong and Jeong [14], Jeong et al. [15], Kang et al. [27], Lee [37], Lee et al. [41] and Hu and Jacobi [49], showing that these correlations present similar results to each other, i.e., Kwong and Jeong's [14] correlation found to fall within the operating range of Lee et al.'s [41] and Hu and Jacobi's [49]. Therefore, the Hu and Jacobi's [49] correlation may be used to design the absorption process (droplet-column pattern flow). However, Jeong et al.'s [15] and Kang et al.'s [27] underestimate the heat transfer due to that the first neglects the effects taken into account by the Prandtl number, and the second carried out the experimental work for absorption processes for a too low degree of purity of ammonia vapor. Also, Fig. 4 shows

**Table 7**
Operational conditions of the ammonia-water ARC.

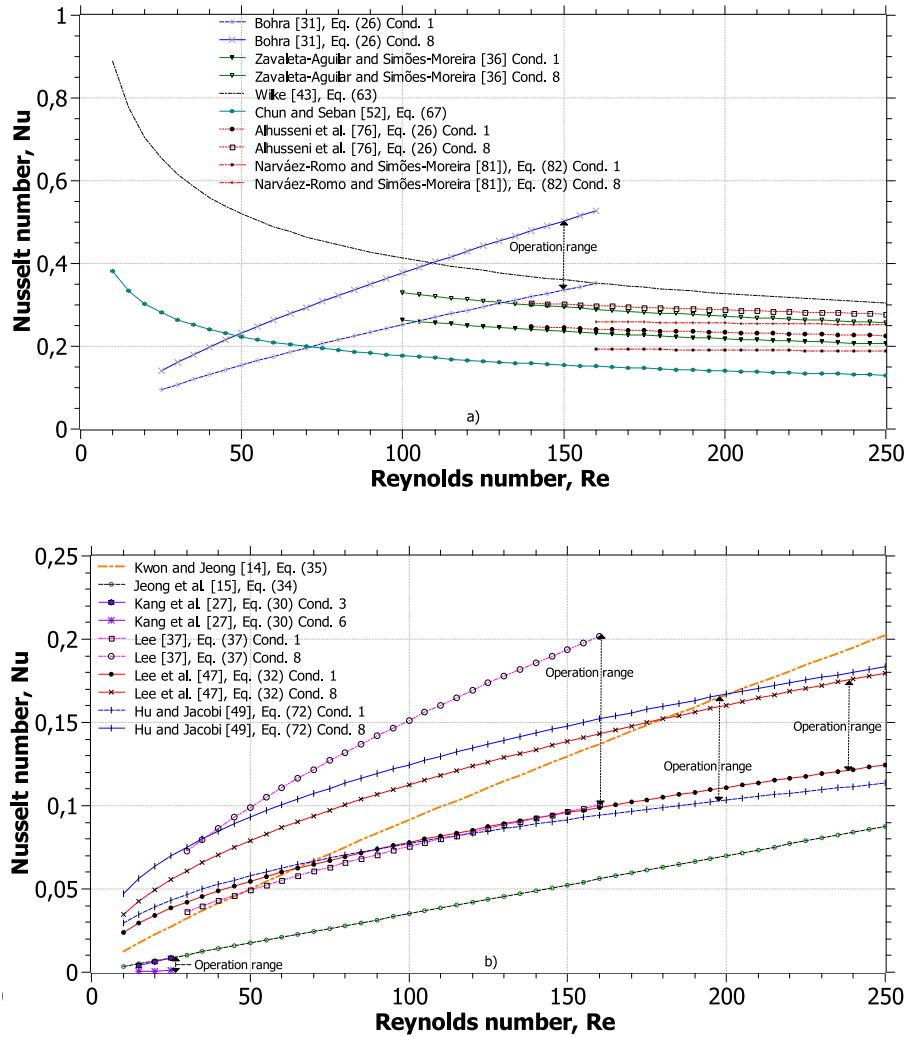| Cond. | $T_{con}$, °C | $T_{eva}$, °C | $T_{gen}$, °C | COP | $P_{abs}$, kPa | $P_{gen}$, kPa | $x_{ss}$, % | $x_{ws}$, % | Pr | Sc |
|---|---|---|---|---|---|---|---|---|---|---|
| 1 | 40 | 7 | 100 | 0.6245 | 554.1 | 1555 | 63.72 | 40.52 | 1.64 | 14.4 |
| 2 | 40 | 7 | 110 | 0.5157 | 554.1 | 1555 | 63.72 | 31.41 | 1.91 | 21.5 |
| 3 | 40 | −20 | 100 | 0.5547 | 190.1 | 1555 | 41.51 | 40.52 | 2.29 | 37.3 |
| 4 | 40 | −20 | 110 | 0.4606 | 190.1 | 1555 | 41.51 | 31.41 | 2.63 | 52.4 |
| 5 | 30 | 7 | 100 | 0.6083 | 554.1 | 1167 | 63.72 | 34.54 | 1.82 | 18.9 |
| 6 | 30 | 7 | 110 | 0.4779 | 554.1 | 1167 | 63.72 | 25.78 | 2.1 | 27.4 |
| 7 | 30 | −20 | 100 | 0.5407 | 190.1 | 1167 | 41.51 | 34.54 | 2.52 | 46.9 |
| 8 | 30 | −20 | 110 | 0.4298 | 190.1 | 1167 | 41.51 | 25.78 | 2.87 | 64.2 |

**Fig. 4.** Nusselt as a function of the Reynolds number for the ammonia-water solution.

**Table 8**
Operational conditions of the lithium bromide-water ARC.

| Cond. | $T_{con}$, °C | $T_{eva}$, °C | $x_{ss}$, % | $x_{ws}$, % | COP | $P_{abs}$, kPa | $P_{gen}$, kPa | $T_{gen}$, 0 °C | $Pr$ | $Sc$ |
|---|---|---|---|---|---|---|---|---|---|---|
| 1 | 40 | 7 | 50 | 62.7 | 0.8659 | 1 | 7.38 | 90.29 | 24.17 | 2101 |
| 2 | 30 | 7 | 50 | 62.7 | 0.883 | 1 | 4.25 | 78.43 | 24.17 | 2101 |

that the Nusselt number may vary between 0.001 and 0.2 for the Reynolds number ranged from 10 to 250 (with an exception of Bohra [31]) for $NH_3 - H_2O$ ARC in refrigeration and air conditioning applications. It is worthwhile to mention that the best performance of the heat transfer is achieved at the lowest vaporization temperature ($T_{eva} = -20$ °C) for all the correlations.

### 6.2. Lithium bromide-water working fluid pair

Vaporization temperature is only evaluated at 7 °C due to refrigerant properties (water). Therefore, this technology is widely used in air conditioning applications. Table 8 shows two typical operational conditions, the second and third columns show the condensation temperature ($T_{con}$) and vaporization temperature ($T_{eva}$), respectively; while $x_{ss}, x_{ws}$ are the strong and weak solution concentrations, respectively. Next, the coefficient of performance (COP), absorption pressure

($P_{abs}$), generation pressure ($P_{gen}$), generator temperature ($T_{gen}$). Finally, the Prandtl number ($Pr$) and Schmidt number ($Sc$) are computed.

Fig. 5 shows the Sherwood number as a function of the Reynolds number, in which the correlations display different behavior for the same operational conditions, i.e., Karami and Farhanieh's [22] and Karami and Farhanieh's [23] correlations show a strong dependence on the Sherwood number as the Reynolds number changes, enhancing the mass transfer as the Reynolds number increases. In contrast, Kim and Ferreira's correlation [32] shows that the increase of the Reynolds number decreases the Sherwood number.

It is worthwhile to mention that the Kim and Ferreira's [32] correlations were obtained experimentally. On the other hand, Babadi and Farhanieh [59] underestimates the Sherwood number as compared with Kim and Ferreira [32], Karami and Farhanieh [22] and Karami and Farhanieh [23].Therefore, Fig. 5 shows that the Sherwood number
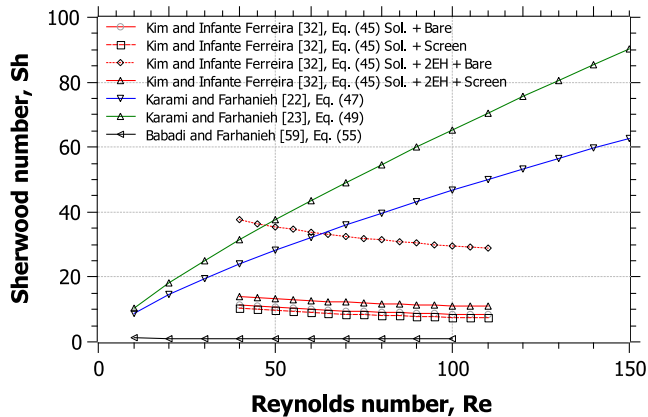
**Fig. 5.** Sherwood number as a function of the Reynolds number for the Lithium bromide-water solution.
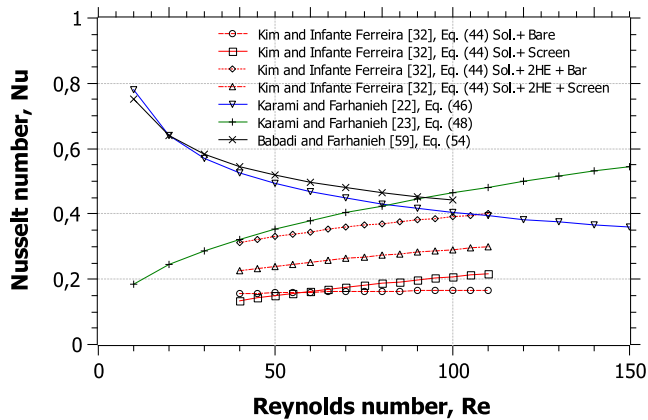


**Fig. 6.** Nusselt number as a function of the Reynolds number for the Lithium bromide-water solution.

may be vary between 0 and 100 for the Reynolds number ranging from 10 to 150 for LiBr-H$_2$O ARC in air conditioning applications.

Finally, Fig. 6 shows the behavior of the Nusselt number as a function of the Reynolds number, in which the heat transfer improves as the Reynolds number increases. Nevertheless, the correlations of Babadi and Farhanieh [59], and Karami and Farhanieh [22] shows an opposite behavior. Nusselt number may be vary between 0.1 and 0.8 for the Reynolds number ranged from 10 to 150 in LiBr-H$_2$O ARC for air conditioning applications.

## 7. Conclusions

In this paper, a critical review of heat and mass transfer correlations for lithium bromide-water and ammonia-water absorption refrigeration machines using falling liquid film technology was presented. The work highlights the following remarks:

1. *Transfer correlations involving ammonia-water working fluid pair:* in absorption processes, the heat and mass transfer enhances as the Reynolds number is increased. Sherwood number may vary from 0.015 to 0.08 for the Reynolds number ranging from 10 to 150. Nusselt number may vary between 0.001 and 0.2 for the Reynolds number ranging from 10 to 250. It was found that correlations carried out for evaporation processes did not apply directly to the absorption process. Moreover, the heat and mass

transfer coefficient was strongly enhanced as the absorption refrigeration cycle achieved vaporization temperatures below 0 °C.

2. *Transfer correlations involving lithium bromide-water working fluid pair:* in absorption processes, there were divergences between theoretical studies (Kim and Ferreira [32], Karami and Farhanieh [22], and Babadi and Farhanieh [59]) and experimental (Kim and Ferreira's [32]) studies. Sherwood number may vary between 0 and 100 for the Reynolds number ranging from 10 to 150, and Nusselt number may vary between 0.1 and 0.8 for the Reynolds number ranged from 10 to 150.

3. Finally, although the technical development of such machines has reached an acceptable maturity for industrial purpose, research is still active as more experimental work and theoretical analysis are necessary.

## References

[1] M. Carmo Elvas, M.I. Perez, S. Carvalho, Making science cooler: Carré's apparatus, in: Int. Conference of ESHS, 2010, pp. 441–449.
[2] M. Yüksel, E. Schlünder, Heat and mass transfer in non-isothermal absorption of gases in falling liquid films, Chem. Eng. Process. Process Intens. 22 (4) (1987) 193–202.
[3] T. Fujita, Falling liquid films in absorption machines, Int. J. Refrig. 16 (4) (1993) 282–294.
[4] J. Castro, C. Oliet, I. Rodríguez, A. Oliva, Comparison of the performance of falling film and bubble absorbers for air-cooled absorption systems, Int. J. Therm. Sci. 48 (7) (2009) 1355–1366.
[5] J.R. Thome, Falling film evaporation: state-of-the-art review of recent work, J. Enhanced Heat Transfer 6 (1999) 263–278.
[6] J.D. Killion, S. Garimella, A critical review of models of coupled heat and mass transfer in falling-film absorption, Int. J. Refrig. 24 (8) (2001) 755–797.
[7] G. Ribatski, A.M. Jacobi, Falling-film evaporation on horizontal tubes - a critical review, Int. J. Refrig. 28 (5) (2005) 635–653.
[8] B. Narváez-Romo, J.R. Simões-Moreira, Falling film evaporation: a qualitative analysis of the distribuition system, in: Proceeding of the Brazilian Congress of Thermal Sciences and Eng. (ENCIT), Belém, 2014.
[9] J.S. Prost, M.T. González, M.J. Urbicain, Determination and correlation of heat transfer coefficients in a falling film evaporator, J. Food Eng. 73 (4) (2006) 320–326.
[10] B. Narváez-Romo, J.R. Sim oes-Moreira, Falling film evaporation: an overview, in: Proceeding of 22nd Int. Congress of Mechanical Eng. (COBEM), Riber ao Preto, 2013, pp. 1–7.
[11] C. Tomforde, A. Luke, Experimental investigations on falling-film absorbers with horizontal tubes a review, in: Int. Refrigeration and Air Conditioning Conference at Purdue, 2012, pp. 1–10.
[12] A.M. Abed, M. Alghoul, M.H. Yazdi, A.N. Al-Shamani, K. Sopian, The role of enhancement techniques on heat and mass transfer characteristics of shell and tube spray evaporator: a detailed review, Appl. Therm. Eng. 75 (2015) 923–940.
[13] R. Taylor, R. Krishna, Multicomponent Mass Transfer, vol. 2, John Wiley & Sons, 1993.
[14] K. Kwon, S. Jeong, Effect of vapor flow on the falling-film heat and mass transfer of the ammonia/water absorber, Int. J. Refrig. 27 (8) (2004) 955–964.
[15] S. Jeong, S.K. Lee, K.-K. Koo, F. Ziegler, et al., Heat transfer performance of a coiled tube absorber with working fluid of ammonia/water/discussion, ASHRAE Trans. 104 (1998) 1577.
[16] G. Florides, S. Kalogirou, S. Tassou, L. Wrobel, Design and construction of a libr–water absorption machine, Energy Convers. Manage. 44 (15) (2003) 2483–2508.
[17] I. Fujita, E. Hihara, Heat and mass transfer coefficients of falling-film absorption process, Int. J. Heat Mass Transfer 48 (13) (2005) 2779–2786.
[18] M.R. Islam, N. Wijeysundera, J. Ho, Evaluation of heat and mass transfer coefficients for falling-films on tubular absorbers, Int. J. Refrig. 26 (2) (2003) 197–204.
[19] T.H. Chilton, A.P. Colburn, Mass transfer (absorption) coefficients prediction from data on heat transfer and fluid friction, Ind. Eng. Chem. 26 (11) (1934) 1183–1187.
[20] E. Treybal Robert, Mass-Transfer Operations, McGraw-Hill Book Company, 1981.
[21] W. Nusselt, Die oberflachenkondesation des wasserdamffes the surface condensation of water, Zetrschr. Ver. Deutch. Ing. 60 (1916) 541–546.

[22] S. Karami, B. Farhanieh, A numerical study on the absorption of water vapor into a film of aqueous LiBr falling along a vertical plate, Heat Mass Trans./ Waerme- Stoff. 46 (2) (2009) 197–207.

[23] S. Karami, B. Farhanieh, Numerical modeling of incline plate LiBr absorber, Heat Mass Trans./Waerme- Stoff. 47 (3) (2011) 259–267.

[24] M. Yüksel, E. Schlünder, Heat and mass transfer in non-isothermal absorption of gases in falling liquid films. Part II: Theoretical description and numerical calculation of turbulent falling film heat and mass transfer, Chem. Eng. Process: Process Intens. 22 (4) (1987) 203–213.

[25] T. Nosoko, a. Miyara, T. Nagata, Characteristics of falling film flow on completely wetted horizontal tubes and the associated gas absorption, Int. J. Heat Mass Transfer 45 (13) (2002) 2729–2738.

[26] C. Ferreira, C. Keizer, C. Machielsen, Heat and mass transfer in vertical tubular bubble absorbers for ammonia-water absorption refrigeration systems, Int. J. Refrig. 7 (6) (1984) 348–357.

[27] Y.T. Kang, A. Akisawa, T. Kashiwagi, Experimental correlation of combined heat and mass transfer for NH$_3$-H$_2$O falling film absorption, Int. J. Refrig. 22 (1999) 250–262.

[28] V. Patnaik, H. Perez-blanco, A study of absorption enhancement by wavy film flows, Int. J. Heat Fluid Flow 17 (1996) (1996) 71–77.

[29] H. Takamatsu, H. Yamashiro, N. Takata, H. Honda, Vapor absorption by LiBr aqueous solution in vertical smooth tubes, Int. J. Refrig. 26 (6) (2003) 659–666.

[30] S. Jani, M.H. Saidi, a.a. Mozaffari, Tube bundle heat and mass transfer characteristics in falling film absorption generators, Int. Commun. Heat Mass 30 (4) (2003) 565–576.

[31] L.K. Bohra, Analysis of Binary Fluid Heat and Mass Transfer in Ammonia-Water Absorption, Ph.D. thesis, Georgia Institute of Technology, 2007.

[32] D.S. Kim, C.a. Infante Ferreira, Flow patterns and heat and mass transfer coefficients of low Reynolds number falling film flows on vertical plates: effects of a wire screen and an additive, Int. J. Refrig. 32 (1) (2008) 138–149.

[33] J. Cerezo, M. Bourouis, M. Vallès, A. Coronas, R. Best, Experimental study of an ammonia-water bubble absorber using a plate heat exchanger for absorption refrigeration machines, Appl. Therm. Eng. 29 (5–6) (2009) 1005–1011.

[34] C. Shi, C. Xu, H. Hu, Y. Ying, Study on falling film generation heat transfer of lithium bromide solution in vertical tubes, J. Therm. Sci. 18 (3) (2009) 241–245.

[35] C. Shi, Q. Chen, T.-C. Jen, W. Yang, Heat transfer performance of lithium bromide solution in falling film generator, Int. J. Heat Mass Transfer 53 (15–16) (2010) 3372–3376.

[36] E. Zavaleta-Aguilar, J. Simões-Moreira, Horizontal tube bundle falling film distiller for ammonia–water mixtures, Int. J. Refrig. 59 (2015) 304–316.

[37] S. Lee, Development of Techniques for In-Situ Measurement of Heat and Mass Transfer in Ammonia-Water Absorption Systems, Ph.D. thesis, Georgia Institute of Technology, 2007.

[38] V.E. Nakoryakov, N.I. Grigoryeva, M.V. Bartashevich, Heat and mass transfer in the entrance region of the falling film: absorption, desorption, condensation and evaporation, Int. J. Heat Mass Transfer 54 (21–22) (2011) 4485–4490.

[39] R.L. Cerro, S. Whitaker, Entrance region flows with a free surface: the falling liquid film, Chem. Eng. Sci. 26 (6) (1971) 785–798.

[40] X. Peng, B. Wang, G. Peterson, H. Ma, Experimental investigation of heat transfer in flat plates with rectangular microchannels, Int. J. Heat Mass Transfer 38 (1) (1995) 127–137.

[41] K.B. Lee, B.H. Chun, J.C. Lee, C.H. Lee, S.H. Kim, Experimental analysis of bubble mode in a plate-type absorber, Chem. Eng. Sci. 57 (11) (2002) 1923–1929.

[42] S. Lee, L.K. Bohra, S. Garimella, A.K. Nagavarapu, Measurement of absorption rates in horizontal-tube falling-film ammonia-water absorbers, Int. J. Refrig. 35 (3) (2012) 613–632.

[43] W. Wilke, (heat transfer to falling liquid films) warmeubertragung an rieselfilme, VDI-Forschungsheft 490 (1962) 36.

[44] X. Hu, A. Jacobi, The intertube falling film: Part 2. Mode effects on sensible heat transfer to a falling liquid film, J. Heat Transfer 118 (3) (1996) 626–633.

[45] J.M. Meacham, S. Garimella, Ammonia-water absorption heat and mass transfer in microchannel absorbers with visual confirmation, ASHRAE Trans. 110(1).

[46] X. Daguenet-Frick, P. Gantenbein, J. Müller, B. Fumey, R. Weber, Seasonal thermochemical energy storage: comparison of the experimental results with the modelling of the falling film tube bundle heat and mass exchanger unit, Renew. Energy 110 (2017) 162–173.

[47] K.B. Lee, B.H. Chun, J.C. Lee, J.C. Hyun, S.H. Kim, Comparison of heat and mass transfer in falling film and bubble absorbers of ammonia water (September 2001) (2002) 191–205.

[48] A. Dorokhov, V. Bochagov, Heat transfer to a film falling over horizontal cylinders, Heat Trans. Soviet Res. 15 (2) (1983) 96–101.

[49] X. Hu, A. Jacobi, The intertube falling film: Part 1-Flow characteristics, mode transitions, and hysteresis, J. Heat Transfer 118 (3) (1996) 616–625.

[50] J. Meacham, S. Garimella, Experimental demonstration of a prototype microchannel absorber for space-conditioning systems, in: Int. Sorption Heat Pump Conference, Shanghai, China, 2002, pp. 270–276.

[51] J.M. Meacham, S. Garimella, Ammonia-water absorption heat and mass transfer in microchannel absorbers with visual confirmation, ASHRAE Trans. 110(1).

[52] K. Chun, R. Seban, Heat transfer to evaporating liquid films, J. Heat Transfer 93 (4) (1971) 391–396.

[53] J. Mitrovic, Influence of tube spacing and flow rate on heat transfer from a horizontal tube to a falling liquid film, in: Proceedings of the 8th Int. Heat Transfer Conference, vol. 4, 1986, pp. 1949–1956.

[54] W. Owens, Correlation of thin film evaporation heat transfer coefficients for horizontal tubes, 1978.

[55] Y. Fujita, M. Tsutsui, Experimental investigation of falling film evaporation on horizontal tubes, Heat Trans.-Japanese Res. 27 (8) (1998) 609–618.

[56] M. Conde, Thermo-physical properties of {NH$_3$ + H$_2$O} mixtures for industrial design of absorption refrigeration equipment, M. Conde Eng. Zurich (2006) 12–15.

[57] S. Jani, Simulation of heat and mass transfer process in falling film single tube absorption generator, Int. J. Sci. Eng. Invest. 1 (3) (2012) 79–84.

[58] L.A. McNeely, Thermodynamic properties of aqueous solutions of lithium bromide, ASHRAE 85 (1979) 413–434.

[59] F. Babadi, B. Farhanieh, Characteristics of heat and mass transfer in vapor absorption of falling film flow on a horizontal tube, Int. Commun. Heat Mass 32 (9) (2005) 1253–1265.

[60] K. Banasiak, J. Kozioł, Mathematical modelling of a LiBrH$_2$O absorption chiller including two-dimensional distributions of temperature and concentration fields for heat and mass exchangers, Int. J. Therm. Sci. 48 (9) (2009) 1755–1764, http://dx.doi.org/10.1016/j.ijthermalsci.2009.01.018.

[61] D. Kim, M.H. Kim, Heat transfer enhancement characteristics for falling-film evaporation on horizontal enhanced tubes with aqueous libr solution, J. Enhanc. Heat Transfer 6 (1) (1999) 61–69.

[62] S. Jani, M.H. Saidi, A. Heydari, A.A. Mozaffari, Second law based optimization of falling film single tube absorption generator, in: ASME 2002 Int. Mechanical Eng. Congress and Exposition, American Society of Mechanical Engineers, 2002, pp. 49–54.

[63] M. Medrano, M. Bourouis, A. Coronas, Absorption of water vapour in the falling film of water-lithium bromide inside a vertical tube at air-cooling thermal conditions, Int. J. Therm. Sci. 41 (9) (2002) 891–898.

[64] L. Hoffmann, I. Greiter, A. Wagner, V. Weiss, G. Alefeld, Experimental investigation of heat transfer in a horizontal tube falling film absorber with aqueous solutions of libr with and without surfactants, Int. J. Refrig. 19 (5) (1996) 331–341.

[65] S.-M. Yih, K.-Y. Chen, Gas absorption into wavy and turbulent falling liquid films in a wetted-wall column, Chem. Eng. Comm. 17 (1–6) (1982) 123–136.

[66] Y. Nagaoka, N. Nishiyama, K. Ajisaka, M. Nakamura, N. Inoue, H. Yabase, E. Hihara, T. Saito, Absorber of absorption refrigerating machine (enhancement of heat and mass transfer in falling film absorbers by surface configuration) (73), na, 1987.

[67] K. Kim, N. Berman, D. Chau, B. Wood, Absorption of water vapour into falling films of aqueous lithium bromide, Int. J. Refrig. 18 (7) (1995) 486–494.

[68] D. Kim, C.I. Ferreira, A gibbs energy equation for libr aqueous solutions, Int. J. Refrig. 29 (1) (2006) 36–46.

[69] R. DiGuilio, R. Lee, S. Jeter, A. Teja, Properties of lithium bromide-water solutions at high temperatures and concentrations–i. Thermal conductivity, ASHRAE Trans. 96 (1) (1990) 702–708.

[70] M. Gierow, A. Jernqvist, Measurement of mass diffusivity with holographic interferometry for H$_2$O-NaOH and H$_2$O-LiBr working pairs, in: Proceedings of the Int. Heat Pump Conference, AES, vol. 31, 1993, pp. 525–532.

[71] E.R. Van-Driest, On turbulent flow near a wall, J. Aeronaut. Sci. 23 (11) (1956) 1007–1011.

[72] N. Goel, D.Y. Goswami, A compact falling film absorber, J. Heat Transfer 127 (9) (2005) 957–965.

[73] N. Goel, D.Y. Goswami, Analysis of a counter-current vapor flow absorber, Int. J. Heat Mass Transfer 48 (7) (2005) 1283–1292.

[74] D. Triché, S. Bonnot, M. Perier-Muzet, F. Boudéhenn, H. Demasles, N. Caney, Experimental and numerical study of a falling film absorber in an ammonia-water absorption chiller, Int. J. Heat Mass Transfer 111 (2017) 374–385.

[75] S.G. Kandlikar, Handbook of Phase Change: Boiling and Condensation, CRC Press, 1999.

[76] K.R. Chun, R. Seban, Performance prediction of falling-film evaporators, J. Heat Transfer 94 (4) (1972) 432–436.

[77] A.A. Alhusseini, K. Tuzla, J.C. Chen, Falling film evaporation of single component liquids, Int. J. Heat Mass Transfer 41 (12) (1998) 1623–1632.

[78] M.W. Shahzada, K.C. Ng, K. Thu, A. Myat, C.W. Gee, An improved film evaporation correlation for saline water at sub-atmospheric pressures, in: AIP Conference Proceedings, 2011.

[79] W. Parken, L. Fletcher, V. Sernas, J. Han, Heat transfer through falling film evaporation and boiling on horizontal tubes, J. Heat Transfer 112 (3) (1990) 744–750.

[80] Z.-H. Liu, Q.-Z. Zhu, Y.-M. Chen, Evaporation heat transfer of falling water film on a horizontal tube bundle, Heat Trans.-Asian Res. 31 (1) (2002) 42–55.

[81] L.-H. Chien, Y.-L. Tsai, An experimental study of pool boiling and falling film vaporization on horizontal tubes in R-245fa, Appl. Therm. Eng. 31 (17) (2011) 4044–4054.

[82] B. Narváez-Romo, J.R. Simões-Moreira, Falling liquid film evaporation in subcooled and saturated water over horizontal heated tubes, Heat Transfer Eng. (2016) 1–57.

[83] B. Leite, Modelagem do absorvedor e do gerador de ciclos de refrigeraç ao por absorç ao de calor com o par NH$_3$-H$_2$O baseados na tecnologia de filme descendente sobre placas inclinadas, (In Portuguese), 2015.